

NASA TECHNICAL NOTE



NASA TN D-7567

NASA TN D-7567

CASE FILE
COPY

PERFORMANCE OF
A HYDROGEN BURNER TO SIMULATE
AIR ENTERING SCRAMJET COMBUSTORS

by William Roger Russin

Langley Research Center

Hampton, Va. 23665

1. Report No. NASA TN D-7567		2. Government Accession No.		3. Recipient's Catalog No.	
4. Title and Subtitle PERFORMANCE OF A HYDROGEN BURNER TO SIMULATE AIR ENTERING SCRAMJET COMBUSTORS				5. Report Date February 1974	
				6. Performing Organization Code	
7. Author(s) William Roger Russin				8. Performing Organization Report No. L-9363	
				10. Work Unit No. 501-04-03-02	
9. Performing Organization Name and Address NASA Langley Research Center Hampton, Va. 23665				11. Contract or Grant No.	
				13. Type of Report and Period Covered Technical Note	
12. Sponsoring Agency Name and Address National Aeronautics and Space Administration Washington, D.C. 20546				14. Sponsoring Agency Code	
15. Supplementary Notes					
16. Abstract <p>Tests were conducted to determine the performance of a hydrogen burner used to produce a test gas that simulates air entering a scramjet combustor at various flight conditions. The test gas simulates air in that it duplicates the total temperature, total pressure, and the volume fraction of oxygen of air at flight conditions. The main objective of the tests was to determine the performance of the burner as a function of the effective exhaust port area (or nozzle throat area), which varied from 15.84 cm² to 53.74 cm². Total pressure was 0.69 MN/m² and total temperature ranged from 1100 K to 2300 K. The conclusions were (1) pressure oscillations of the chugging type were reduced in amplitude to ±2 percent of the mean pressure level by proper sizing of hydrogen, oxygen, and air injector flow areas; (2) combustion efficiency remained essentially constant as the exhaust port area was increased by a factor of 3.4; (3) the mean total temperature determined from integrating the exit radial gas property profiles was within ±5 percent of the theoretical bulk total temperature; (4) the measured exit total temperature profile had a local peak temperature more than 30 percent greater than the theoretical bulk total temperature; and (5) measured heat transfer to the burner liner was 75 percent of that predicted by theory based on a flat radial temperature profile.</p>					
17. Key Words (Suggested by Author(s)) Burner Scramjet Burner performance			18. Distribution Statement Unclassified - Unlimited STAR Category 28		
19. Security Classif. (of this report) Unclassified		20. Security Classif. (of this page) Unclassified		21. No. of Pages 56	22. Price* \$3.50

PERFORMANCE OF A HYDROGEN BURNER TO SIMULATE AIR ENTERING SCRAMJET COMBUSTORS

By William Roger Russin
Langley Research Center

SUMMARY

Tests were conducted to determine the performance of a hydrogen burner used to produce a test gas that simulates air entering a scramjet combustor at various flight conditions. The test gas simulates air in that it duplicates the total temperature, total pressure, and the volume fraction of oxygen of air at flight conditions. The main objective of the tests was to determine the performance of the burner as a function of the effective exhaust port area (or nozzle throat area), which varied from 15.84 cm² to 53.74 cm². Total pressure was 0.69 MN/m² and total temperature ranged from 1100 K to 2300 K. The conclusions were (1) pressure oscillations of the chugging type were reduced in amplitude to ± 2 percent of the mean pressure level by proper sizing of hydrogen, oxygen, and air injector flow areas; (2) combustion efficiency remained essentially constant as the exhaust port area was increased by a factor of 3.4; (3) the mean total temperature determined from integrating the exit radial gas property profiles was within ± 5 percent of the theoretical bulk total temperature; (4) the measured exit total temperature profile had a local peak temperature more than 30 percent greater than the theoretical bulk total temperature; and (5) measured heat transfer to the burner liner was 75 percent of that predicted by theory based on a flat radial temperature profile.

INTRODUCTION

A valuable approach to determination of the characteristics of hydrogen-fueled scramjets (supersonic-combustion ramjets) is basic combustion experiments (refs. 1 to 6) combined with theoretical analyses of the flow and combustion phenomena. This approach is believed to minimize the cost of achieving a good first design for the complete engine.

In order to conduct these ground-based combustion experiments, a device must produce a test gas that simulates the air that would enter the combustor component at various flight conditions. The test-gas simulation of the air includes the duplication of enthalpy, oxygen volume fraction, and total pressure that would be encountered in flight. Among the devices generally used to produce the test gas are arc heaters, ceramic stor-

age heaters, and combustion burners. This report is concerned with performance tests made with one of the latter – a hydrogen burner in which the air is directly heated by flames and oxygen added to maintain the oxygen volume fraction equal to that of air (0.2095). Although the burner engineering design (ref. 7) was first thought to be satisfactory, additional tests were necessary to document its characteristics as the nozzle throat area was increased beyond the design. A larger throat area is desired for the burner nozzle so that combustion experiments more representative of combustors for flight scramjets can be tested, and also to obtain larger exit flows whose properties can be more easily measured in detail.

The purpose of this investigation was to determine the performance of the hydrogen burner as the nozzle throat area increased by factors up to 3.4. The performance characteristics studied were (1) pressure oscillations, (2) combustion efficiency, (3) heat transfer to burner wall, and (4) total temperature and pressure profiles at the burner exit. In these tests the total temperature range was 1100 K to 2300 K. The range of effective throat areas was 15.84 cm² to 53.74 cm². Instead of a contoured convergent-divergent nozzle, an uncooled, mild steel plate with a circular hole (exhaust port) in its center was used to exhaust the test gas from the burner. Thus, throat area was increased between tests by simply boring a larger hole in the plate. There is no reason to believe that the performance results reported herein would have been any different had a contoured convergent-divergent nozzle been used instead.

SYMBOLS

A	geometric area, meters ²
C _d	discharge coefficient, dimensionless
C _f	friction coefficient
C _p	specific heat, J/kg-K
D	exhaust port diameter, centimeters
D _e	hydraulic diameter or gap height, meters
F	profile factor, dimensionless (see appendix C)
F _{HL}	heat-loss fraction, dimensionless (see eq. (C8))

H	enthalpy, J/kg
$H_{\text{ref}} = \frac{1}{2}(H_t - H_{\text{sat}})$	
h	heat-transfer film coefficient, J/sec-K-m ²
K	thermal conductivity, J-m/kg-K
M	Mach number
m	mixture ratio dimensionless, $\dot{w}_{\text{H}_2} / (\dot{w}_{\text{O}_2} + \dot{w}_{\text{air}})$
M	molecular weight
N_{Pr}	Prandtl number
N_{St}	Stanton number
p	pressure, N/m ²
\bar{p}_{oa}	oscillation amplitude percentage of the mean pressure (see eq. (1))
\dot{Q}_{adj}	adjusted bulk heat-transfer rate, J/sec
Q_{R}	heat release per mass of hydrogen, 1.338×10^8 J/kg
\dot{q}	heat-transfer flux, J/m ² -sec
R	universal gas constant, 8314 J/kmol-K
r	radial position from center line, meters
T	temperature, K
V	velocity, m/sec
\dot{w}	flow rate, kg/sec

w_{adj}	adjusted flow rate, kg/sec
x	axial position, meters
y	wall thickness, meters
α	mass fraction, dimensionless
γ	ratio of specific heats, dimensionless
η_c	combustion efficiency, dimensionless
μ	viscosity, N-sec/m ²
ν	kinematic viscosity, μ/ρ
ρ	density, kg/m ³
τ	heat release delay, sec

Superscript:

f refers to profile factor, F

Subscripts:

b bulk

f final, frozen

g test gas

i initial, integration step number (see appendix D)

J thermocouple junction

l liquid water

m measured

max	maximum
min	minimum
ref	reference
s	supply
sat	water saturation
t	burner stagnation conditions
w	wall

APPARATUS AND PROCEDURE

Hydrogen Burner

The burner is schematically shown in figure 1. Dry air is supplied at 4.14 MN/m^2 from blowdown tanks. Hydrogen and oxygen are supplied from high-pressure trailers and are regulated to a maximum supply pressure of 4.96 MN/m^2 . Combustion products are exhausted to the atmosphere through a bellmouthed duct system. (For heater design details, consult ref. 7.) Usually, a contoured convergent-divergent nozzle is used for combustor tests, but in the present tests the test gas was exhausted through an uncooled nozzle plate of mild steel with a central circular exhaust port. A two-stage centrifugal pump supplied cooling water for the burner at $62.7 \text{ m}^3/\text{hr}$ and 3.45 MN/m^2 .

Instrumentation and Data Acquisition

Hydrogen, oxygen, and air gas flow rates were measured using ASME sharp-edge orifice meters. The pressure at each flow meter, the burner total pressure, burner liner temperatures, and water-cooling flow rates were recorded digitally on magnetic tape by a computer-controlled 200-channel data acquisition system. Burner total pressure was assumed to equal the average measured liner-wall static pressures since the static and total pressure are within 0.5 percent of each other in this low Mach number flow. Strain-gage pressure transducers were used to measure pressure oscillations. Oscillations of the burner total pressure and the hydrogen differential and air differential pressures at their respective flow measurement orifice plates were recorded with an oscillograph. Burner-cooling-water initial and final temperatures were recorded on a dual-pen chart recorder.

Traverse Probe

As seen in figure 2, the traverse probe measured both pitot pressure and gas temperature downstream of the throat. Probe cooling water enters through the hollow support shaft and flows through an annular passage to the probe tips where it is turned back and exhausted from behind the tips. Some of the water flows through another annular passage on the back side of the pitot tube, issues from small holes, and provides continuous transpiration cooling. Tubing (0.317-cm diameter) containing the thermocouple leads was brazed to the cooling tube which dumped water at the base of the probe assembly. The thermocouple bead material was Ir/Ir-0.40 Rh or Pt/Pt-0.13 Rh and was formed from 24-gage wire. The probe was traversed across the diameter of the nozzle plate exhaust port with the two probes moving in the same plane, the pitot probe preceding the thermocouple probe.

Burner Thermocouple Probe

As shown in figure 3 the burner thermocouple probe was located in relatively low velocity flow upstream of the throat. The junction materials were the same as previously described but, unlike the traverse probe, it was cooled by recirculated water. Both the traverse and the burner probe outputs were recorded on an oscillograph.

General Test Procedure

After establishing the desired air flow, the ignitor was lit. A hydrogen flow of about 20 percent of the total required for the test was supplied to the burner. With this amount of hydrogen burning initially, the hydrogen flow was increased to the desired level and the required oxygen was supplied to the burner. Three seconds were required to achieve steady-state pressure in the burner, and 20 seconds to reach steady-state cooling water temperature. Results from several tests of 30 seconds duration were used to establish the transient characteristics of burner operation.

Test Conditions

The exhaust port and the three gas injector sizes for corresponding test numbers are given in table I. Each injector size changed with exhaust port size to keep the injector pressure drop small. Although a large injector pressure drop would tend to isolate gas feed lines from burner pressure oscillations, the necessity to operate the burner at high pressure (3.1 MN/m^2) for basic combustion tests with a limited gas supply pressure (4.14 MN/m^2) makes operation with a small pressure drop mandatory. The range of injector sizes examined in these tests was intended to bracket the minimum feasible pressure drop. The nominal burner pressure for these tests was 0.69 MN/m^2 and the total temperatures ranged from 1100 K to 2300 K for each nozzle size. In order to maintain

TABLE I.- BURNER CONFIGURATIONS TESTED

Test	Exhaust port diameter, cm	Injector diameter, cm		
		H ₂	O ₂	Air
46	4.83	0.259	0.450	1.59
48	5.64	.259	.450	1.59
49	6.04	.259	.450	1.59
50	6.04	.307	.531	1.83
51	6.40	.307	.531	1.83
52	7.12	.307	.531	1.83
53	7.12	.396	.635	2.19
54	8.13	.396	.635	2.19
55	8.13	.396	.635	2.34
56	8.89	.396	.635	2.34
71 to 75	8.89	.470	.742	2.79

the oxygen volume fraction to that of air, the ratio of the hydrogen mass flow to oxygen mass flow rate to the burner was constant at 0.0823. See appendix A for calculation procedures to estimate supply pressures for desired burner stagnation conditions.

RESULTS AND DISCUSSION

Stability

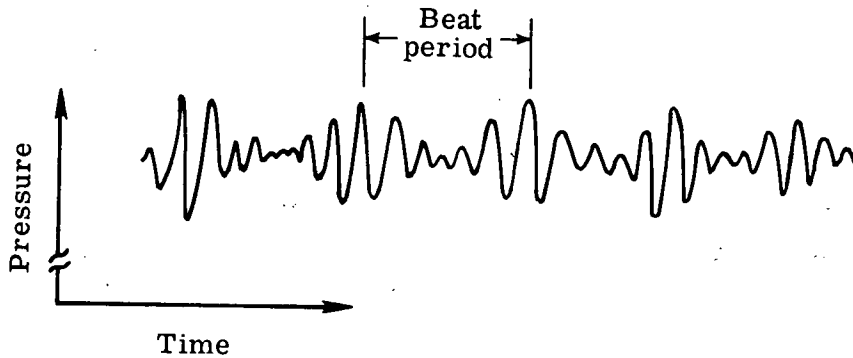
The burner pressure oscillations encountered were of the chugging type described in rocket motor literature. (See ref. 8 (p. 30) and ref. 9.) The objective was to reduce the oscillation amplitude to an acceptable level (defined later). The pressure oscillation frequency changed with the test conditions, but for any given test, all the measured pressure oscillations were sinusoidal and at the same frequency. The variation of frequency with exhaust port diameter is given in figure 4. In the burner combustion chamber the frequency of the driving force was found to vary with the speed of sound in the burner and in figure 4 this effect was eliminated in the ordinate. The reason for the existence of a minimum is not known although the bulk of the data show an increase from the minimum as the exhaust port diameter increases, that is, as the mean velocity of the test gas in the burner increases.

Oscillation amplitude percentage of the mean pressure, frequency beat period, and injector pressure drop fraction are used in the subsequent discussion of the stability results and are defined herein. The first parameter, the oscillation amplitude percent-

age \bar{p}_{oa} of the mean pressure, is computed as follows:

$$\bar{p}_{oa} = \pm \left[\frac{p_{\max} - p_{\min}}{p_{\max} + p_{\min}} \right] (100) \quad (1)$$

This parameter quantizes the pressure oscillation amplitude and will facilitate comparison of the data. In equation (1) the bracketed quantity is evaluated in one of the following ways: (1) when no beating occurs the quantity is averaged over ten cycles or (2) when beating occurs the quantity is evaluated at only the maximum amplitude in each beat period and is averaged over 10 beat periods. The second parameter of interest is the period associated with the beat frequency of the pressure oscillations. (See refs. 10 and 11.) The beat period is illustrated in sketch (a):



Sketch (a)

The beat period becomes infinite when the driving force has the same frequency as the resonating component in the system. This fact was used to determine experimentally the natural frequency of the component as will be explained later. The third parameter is the injector pressure drop fraction which indicates the resistance at the injector to upstream propagation of pressure disturbances and is defined as

$$\text{Pressure drop fraction} = \frac{p_s - p_t}{p_s} \quad (2)$$

where p_s is the gas supply pressure and p_t is the burner total pressure. When the pressure drop fraction is small, there is little resistance and the upstream and downstream regions are closely coupled to each other. But as the pressure drop fraction increases, the resistance increases and continues to increase until the velocity of the fluid emerging from the injector is sonic. For this condition the upstream region is completely decoupled from the downstream region.

Figures 5 to 13 show the measured values of beat period, pressure oscillation frequency, oscillation amplitude percentage (\bar{p}_{oa}), and injector pressure drop fraction as a function of mixture ratio; exhaust port diameters range from 4.83 cm to 8.89 cm. Pressure oscillation frequency varies with mixture ratio like the speed of sound in the burner varies with the temperature as seen by comparing the theoretical slope of sound speed and the data plotted in figures 5 to 13. The comparison is reasonably good although other influences on this frequency variation are evident in the data. A natural frequency of 14 to 16 Hz was determined by noting the pressure oscillation frequency at which the beat period went to very large values (denoted by dashed lines in figs. 5 to 13). Beats did not occur in all tests because the oscillation frequency at those times was not close to the natural frequency.

If it is assumed that the natural frequency is an acoustic mode of the organ pipe kind, then a length can be computed and compared with the lengths of the various gas feed lines to identify the resonating system component. The air feed line was identified as the probable resonating component, since it had a computed natural frequency of either 10 or 20 Hz, depending on whether the feed line was assumed to have one end open or both ends open. It was also noted (see figs. 7 to 13) that, as the air pressure drop fraction decreased, the magnitude of the burner total-pressure oscillations (\bar{p}_{oa}) increased because of increased coupling between the air line and burner. This result again points to the air feed line as the resonating component.

For an exhaust port diameter of 7.12 cm (see figs. 8 and 9) the change from small to large injector flow areas was accompanied by an increase in \bar{p}_{oa} in the hydrogen and air feed lines, which followed the trend of the pressure oscillations in the burner. This condition suggests that the reduced pressure drops at the injectors cause increased coupling between the burner and the feed lines. For an exhaust port diameter of 8.13 cm (see figs. 10 and 11), an increase in air injector flow area was accompanied by a similar increase in the burner pressure oscillation at a given mixture ratio. Again this condition indicates a coupling between the air feed line and the burner.

It is interesting to note that a maximum in the burner \bar{p}_{oa} occurs in figures 6, 7, 8, and 10 and might have occurred in other tests if the mixture ratio range had been extended to higher values. The maximum probably occurs because of two counteracting effects; namely (1) decreasing air pressure drop caused increased coupling between the air feed line and the burner; and (2) increasing hydrogen pressure drop caused decoupling of the fuel supply from the burner. At low mixture ratios the first phenomenon predominates, and at high values the second predominates. The result is the occurrence of a maximum.

Usually an increase in exhaust port diameter was accompanied by an increase in burner total-pressure oscillation amplitude. But satisfactory stability (defined as pres-

sure oscillations within an acceptable \bar{p}_{oa} of ± 2 percent) was achieved whenever the air pressure drop fraction was equal to or greater than the hydrogen and oxygen pressure drop fractions. Based on these results, satisfactory stability can be achieved by selection of the injector flow areas to provide this pressure drop relationship at the desired mixture ratio or total temperature of the burner.

Combustion Efficiency

Combustion efficiency (defined as the mass flow of hydrogen reacted divided by the mass flow of hydrogen injected) is calculated from measured flow rates, coolant heat loss, and exhaust port diameter using heat and mass balance equations. (Details are in appendix B.) Computed combustion efficiencies for these tests are shown in figure 14. As pointed out in appendix B, the combustion efficiency was forced to equal 100 percent for the smallest exhaust port diameter at low total temperatures by selection of the exhaust port discharge coefficient, which then was presumed to remain constant. Note that for all port sizes the combustion efficiency decreases with increasing total temperature. However, several factors were neglected in this analysis: (1) heat loss to the nozzle plate, whose internal surface area is 5 percent of the burner liner area, and (2) effects on discharge coefficient of changes in Reynolds number, of changes in radial temperature gradient and of changes due to thermal expansion of the nozzle plate. The most important conclusion is that no appreciable change in combustion efficiency occurred over the total temperature range of 1300 K to 2400 K and indicated that no gross degradation of combustion efficiency occurred as the exhaust port area and mass flow rate increased by a factor of 3.4.

Heat Transfer

The results of the heat-transfer analysis described in appendix C are presented here. Figures 15 and 16 show the embedded-wall-thermocouple temperature distribution along the burner liner for two exhaust port diameters. The peaks and valleys occurred throughout the tests and are probably the result of differing thermal contact between the thermocouple and the liner wall. For a large nozzle throat size (fig. 16) the temperature difference between the wall thermocouples and the bulk water temperature is nearly constant in contrast to a small throat size (fig. 15). This condition indicates that the heat-transfer rate, which is proportional to this temperature difference, is also nearly constant along the liner for the larger nozzle throat size.

A map of the measured bulk heat-transfer rate (adjusted for slight variations in burner total pressure) is shown in figure 17. Note that the bulk heat-transfer rate for a constant total temperature does not increase as $(\dot{w})^{0.8}$ according to the theory (eq. (C7)), but rather at a slower rate. This nearly constant bulk heat-transfer rate causes the heat-loss fraction to decrease rapidly with increasing flow rate (eq. (C8)) as

shown in figure 18. Theory predicts that the heat-loss fraction should decrease as $(\dot{w})^{-0.2}$ which was determined as follows:

$$\left. \frac{\dot{q}A_w}{\dot{w}_{H_2} Q_R} \right|_{T_t=\text{Constant}} \propto \frac{(\dot{w})^{0.8}}{\dot{w}} \propto (\dot{w})^{-0.2} \quad (3)$$

by obtaining \dot{q} from equation (C7) and by using the following proportionality:

$$\dot{w}_g \propto \dot{w}_{H_2}$$

at a fixed total temperature. The slope of the theory is compared with the data in figure 18. The rapid decrease in measured heat-loss fraction for low mass flow rates can be explained as a temperature profile effect which increases with increasing nozzle throat size and decreasing gas total temperature. (See "Temperature Profile" section for further discussion.)

The decrease in hot-gas-side heat-transfer due to a temperature profile effect can be represented by a profile factor F defined in appendix C. Figure 19 shows the profile factor required to get the hot-gas-side heat-transfer theory (eq. (C7) and fig. 17) to match the measured bulk heat transfer. There is a minimum value of the profile factor which corresponds to a maximum in radial temperature profile gradient. (See "Temperature Profile" section for further discussion). At this value of the profile factor, the heat transfer was 75 percent of that predicted by the theory for no radial temperature gradient, that is, $F = 1$.

Temperature Profile

Total temperatures in the burner measured by use of the burner thermocouple probe (fig. 3) are compared with burner theoretical bulk total temperatures in figure 20. The difference between the theoretical bulk and the measured total temperature is a result of radial temperature gradients in the test gas flow. This difference is larger for the oxygen-replenishment case than for the no-oxygen-replenishment case, as will be explained later. Note that some of the tests reported in this section of the report were for no oxygen replenishment; that is, only hydrogen and air were injected into the burner and hence the oxygen volume fraction of air was not duplicated, but rather, was deficient. Above 1940 K, the softened Pt/Pt-0.13 Rh thermocouple may have structurally failed, and bent downstream into the wake of the cooled probe support; thereby, a lower temperature was indicated than that recorded by the unbent Ir/Ir-0.40 Rh thermocouple.

The theoretical total temperature curve for the test gas having oxygen replenishment is shown in figure 20 and is compared with a hydrogen-air curve (from ref. 12), that

has no oxygen replenishment; both curves are for zero heat loss. In this comparison, by holding mixture ratio constant, the test-gas total temperature is lower than that of the hydrogen-air mixture. This condition occurs because in going from the hydrogen-air mixture to the test-gas mixture, oxygen replaces nitrogen. The molar specific heat of oxygen is greater than that of nitrogen and is responsible for the indicated 40 K to 50 K difference.

To explain the difference between the theoretical and measured burner total temperatures in figure 20, consider the following. Total-temperature and pressure radial profiles were obtained downstream of the burner exhaust port where the burner was operated at a low bulk temperature of 1470 K to avoid melting the thermocouples at the flow center line. The reason for the difference between measured and theoretical temperatures can be seen by noting the high temperatures (more than 30 percent greater than the mean) in the center of the flow as shown in figures 21 and 22. It appears that the burner thermocouple probe was reading the local temperature near the peak of the radial temperature profile inside the burner. Profile shapes are somewhat skewed – probably because of unsymmetrical injection and mixing. Essentially, the same temperatures were obtained from the two types of thermocouples, as can be seen in figure 22. This result is important as a justification for using Ir/Ir-0.40 Rh thermocouples in high-temperature oxygen-rich supersonic flow. (Also, see ref. 5.) To check the consistency of the measured profiles with the theoretical bulk total temperature, a mean temperature was obtained from the corrected total-temperature profiles with the integration technique described in appendix D. These mean values were compared with the theoretically determined bulk values and were found to agree within 5 percent. (See fig. 20.)

The shape of the temperature profile can be explained in terms of the location of the hydrogen injectors in the burner. The hydrogen injector ring of 12 orifices was located on a circumference that divided the air passage so that one-fourth of the air flow area was inside the ring and three-fourths outside. If it is assumed that of the hydrogen injected, half mixes inside the hydrogen ring and half outside, then higher local mixture ratios will be found near the center line and lower ratios near the wall. The initial mixture ratio profile just described would produce an initial temperature profile like that shown in figure 23, where a comparison is made with the measured profile. Note that the profiles have similar center-line temperatures. Figure 23 suggests that the temperature profile could be improved by relocating the hydrogen injector ring.

Variation of the peak of the temperature profile with nozzle throat size and bulk mixture ratio can be obtained by using the burner thermocouple probe data, which were obtained over a large range of burner bulk total temperature. The only complete profile was measured for a total temperature of 1470 K. This burner probe data is shown in figure 24, where it can be seen that profile effects are largest at a mixture ratio of 0.017. Compare this result with figure 19 where a maximum in profile effect was also found, but

at a different mixture ratio. It was noted that profile effects became more severe as air velocity at the hydrogen injectors increased; that is, for larger exhaust port size and/or lower mixture ratios.

CONCLUDING REMARKS

Performance tests were conducted by use of a hydrogen burner which produces a test gas that simulates air entering a scramjet combustor at flight conditions. The test objective was to determine the burner performance as the exhaust port area was increased by factors up to 3.4 and the results are summarized as follows: (1) pressure oscillations of the chugging type were reduced in amplitude to ± 2 percent of the mean pressure level by proper sizing of hydrogen, oxygen, and air injector flow areas; (2) combustion efficiency remained essentially constant as the exhaust port area was increased by a factor of 3.4; (3) the mean total temperature determined from integrating the exit radial gas property profiles was within ± 5 percent of the theoretical bulk total temperature; (4) the measured exit total-temperature profile had a local peak temperature more than 30 percent greater than the theoretical bulk total temperature; and (5) measured heat transfer to the burner liner was 75 percent of that predicted by theory based on a flat radial temperature profile.

Langley Research Center,
National Aeronautics and Space Administration,
Hampton, Va., January 22, 1974.

APPENDIX A

ESTABLISHMENT OF DESIRED BURNER STAGNATION CONDITIONS

If the burner heat loss fraction (see appendix C) is known, the flow rates of hydrogen, oxygen, and air can be determined from figures 25, 26, and 27 for the test conditions reported herein. With the individual gas flow rates and using figures 28, 29, and 30, the injector pressure drop fraction (eq. (2)) and subsequently the gas supply pressures can be found. The discharge coefficient for the injectors was assumed to be 0.80.

APPENDIX B

COMPUTED COMBUSTION EFFICIENCY

The combustion efficiency analysis of the burner consisted of performing an energy balance on the burner while satisfying flow continuity. The data required as input for the one-dimensional computer program written to perform this analysis included coolant flow rates and temperatures, burner total pressure, gas flow rates and temperatures, and the nozzle throat area. In the program the initial value of the enthalpy is found by calculating the enthalpy of the mixture from the flow rates and temperatures of the input gases and then subtracting the enthalpy lost to the cooling water. From this value of enthalpy, the measured total pressure, and the assumption that the mixture is in thermal and chemical equilibrium, the stagnation properties of the mixture are found. By assuming isentropic expansion to sonic speed and using the known throat area, the mass flow is calculated. Iteration of this procedure is carried out by varying the combustion efficiency until the input and output flows match.

The combustion efficiency is defined as

$$\eta_c = \frac{\text{Mass flow of hydrogen reacted}}{\text{Total injected hydrogen mass flow}}$$

In the analysis the iteration on combustion efficiency is accomplished by allowing only a fraction η_c of the total injected hydrogen to react in an equilibrium mixture. The remaining fraction is added at ambient temperature to the equilibrium mixture and the temperature and density are recalculated.

The term "combustion efficiency" as used in this report requires some qualification because, although the geometric area of the exhaust port was known, the flow discharge coefficient was not. Analysis of unreported data, using a contoured convergent-divergent nozzle with a flow discharge coefficient of essentially unity, yielded a combustion efficiency of unity. Since the flow area of the exhaust port with a diameter of 4.83 cm was equal to the throat area of the contoured nozzle, the analysis for that port diameter was forced to yield $\eta_c = 1.00$ at a total temperature of 1720 K by using a discharge coefficient of 0.866. This value for the discharge coefficient was used for all data presented in this report.

APPENDIX C

HEAT-TRANSFER ANALYSIS

Average Measured Burner-Liner-Wall Heat Flux

Wall heat flux was calculated from the measured coolant flow rate and temperature change. Water temperatures were corrected to steady-state values for all tests by using the curve in figure 31, which was established by using only the longer test time data. The heat transferred to the cooling water was assumed to be transmitted only through the burner liner wall; whereas, heat transfer between the coolant and surroundings was considered to be negligible. It was also assumed that the coolant was well mixed at the pipe section where the water temperatures were measured. The average heat flux was obtained from the following equation:

$$\dot{q}_m = \frac{[\dot{w}C_p(T_f - T_i)]_{\text{water}}}{A_w} \quad (\text{C1})$$

For the theoretical calculation the steady-state heat-transfer model assumed is shown in figure 32.

Coolant-Side Heat-Transfer Theory

Turbulent heat transfer is related to the skin friction through a modified Reynolds analogy. The form of the analogy used is due to Colburn (see ref. 13, p. 346, eq. (8-18)) and is stated as

$$N_{St} = \frac{h}{\rho V C_p} = \frac{C_f}{2N_{Pr}^{2/3}} \quad (\text{C2})$$

and by definition

$$C_f = \frac{\tau}{\frac{1}{2}\rho V^2} \quad (\text{C3})$$

An expression for the shear stress τ based on the average water velocity (see ref. 14, p. 564) is stated as

$$\tau = 0.03955\rho V^{7/4} \nu^{1/4} D_e^{-1/4} \quad (\text{C4})$$

APPENDIX C – Continued

Combining equations (C2), (C3), and (C4) and solving for the film coefficient gives

$$h = 0.03955 \frac{C_p(\rho V)^{3/4} \mu^{1/4}}{N_{Pr}^{2/3} D_e^{1/4}} \quad (C5)$$

Because thermocouple temperature measurements were made in the burner-liner-wall, it was of interest to compute these temperatures for comparison with the data. The data are corrected to steady-state values by using the curve in figure 33. The theoretical computations were made by use of the following equation:

$$T = \dot{q}_m A_w \left(\frac{y}{K_w} + \frac{1}{h_l} \right) + T_b \quad (C6)$$

Wall Thermocouple Data

As mentioned earlier (see "Heat Transfer" in section "Results and Discussion"), the measured wall temperature distribution along the liner has peaks and valleys. (See fig. 16.) Varying thermal contact between the thermocouples and the wall may explain this situation. Because the theory assumed good thermal contact, the theoretical temperature was compared with the average of the peak temperatures; the reason is that the thermocouples with the best thermal contact should register the highest temperatures.

The results of these calculations are shown in figure 34 for D_e equal to both hydraulic diameter and gap height of the annular water passage. The theory using annular gap height shows the best agreement with the data probably because the annular flow approaches channel flow locally, that is, the ratio of outer to inner diameter of 1.05 is close to 1. Hence the Reynolds number should be based on the gap height rather than on the hydraulic diameter.

Hot-Gas-Side Heat-Transfer Theory

The following equation, a modification of the one in reference 7, was used to evaluate the hot-gas-side heat-transfer rate:

$$\dot{q} = 0.023 \frac{(\dot{w}/A)^{0.8} (T_t/T_{ref})^{0.8} (\mu_{ref})^{0.2} (H_t^f - H_{sat})}{D_e^{0.2} N_{Pr}^{0.67}} \quad (C7)$$

where H_t^f corresponds to $T_t^f = FT_t$ and where T_{ref} corresponds to

APPENDIX C – Concluded

$H_{\text{ref}} = \frac{1}{2}(H_t + H_{\text{sat}})$ of the reference. There were two modifications required to adapt the referenced equation to the physical situation and yield equation (C7). In the first modification the wall surface temperature was replaced by the condensate surface temperature, which was taken to equal the saturation temperature of water. In the second modification the bulk gas total temperature was reduced by a profile factor F . The theory with these modifications predicted the measured heat transfer where values of F varied from 0.83 to 0.93. These F values are reasonable when the temperature profiles measured are considered. (See "Temperature Profile" section.)

Heat-Loss Fraction

An important parameter is the burner heat loss fraction or fraction of theoretical heat release that is lost to the coolant which is defined as

$$F_{\text{HL}} = \frac{\left[\dot{w} C_p (T_f - T_i) \right]_{\text{water}}}{\dot{w}_{\text{H}_2} Q_R} \quad (\text{C8})$$

Knowledge of this fraction is necessary in establishing the desired burner stagnation conditions described in appendix A.

APPENDIX D

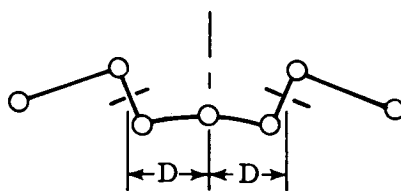
TEMPERATURE PROFILE DATA REDUCTION

The burner thermocouple probe and traversing thermocouple probe measurements are presented both as thermocouple junction temperatures and as total temperatures where the latter are defined to be junction temperatures corrected for convective, conductive, and radiative losses. The traversing probe measurements of both pitot pressure and temperature were used to obtain the Mach number and total temperature profiles using a nozzle exhaust gas flow model shown in figure 35. From these profiles the integrated mass-weighted total temperature was calculated by use of the following procedure.

Temperature Profile Integration Technique

The steps in the technique for temperature profile integration are as follows:

(1) Center the pitot profile as in sketch (b) by using the position of the shocks nearest the center line.



Sketch (b)

(2) Shift the temperature profile the same amount as was required to center the pitot profile.

(3) By using local values of pitot pressure and calculated values of local total pressure including shock losses, obtain the Mach number from isentropic flow relations.

(4) Obtain the local total temperature by correcting the local thermocouple junction temperatures for convective, conductive, and radiative losses.

(5) Determine the local gas composition, molecular weight, specific heat, and ratio of specific heats by assuming the O_2 volume fraction to be 0.2095 and the combustion efficiency to be unity.

(6) From the local Mach number, determine static pressure and static temperature, by use of isentropic flow relations.

APPENDIX D – Concluded

(7) Compute the local density on the profile from

$$\rho = \frac{pM}{RT}$$

(8) Compute the local velocity on the profile from

$$V = M\sqrt{\gamma(R/M)T}$$

(9) Select the integration limits at the edges of the pitot pressure profile 1/2 probe diameter in toward the center line from the point that is just atmospheric pressure.

(10) Integrate the equations for total flow rate, bulk total temperature, and total hydrogen flow rate under the entire profile by using the trapezoidal rule.

Integration Equations

The following integration equations are used:

Total flow rate:

$$\dot{w} = \frac{\pi}{2} \sum_{i=0}^{i_{\max}-1} \left\{ \left[(r_{i+1})^2 - (r_i)^2 \right] \left[\frac{(\rho V)_{i+1} + (\rho V)_i}{2} \right] \right\}$$

Bulk total temperature:

$$T_{t,b} = \frac{\sum_{i=0}^{i_{\max}-1} \left\{ \left[(r_{i+1})^2 - (r_i)^2 \right] \left[\frac{(\rho VC_{p,f} T_t)_{i+1} + (\rho VC_{p,f} T_t)_i}{2} \right] \right\}}{\sum_{i=0}^{i_{\max}-1} \left\{ \left[(r_{i+1})^2 - (r_i)^2 \right] \left[\frac{(\rho VC_{p,f})_{i+1} + (\rho VC_{p,f})_i}{2} \right] \right\}}$$

Total hydrogen flow rate:

$$\dot{w}_{H_2} = \frac{\pi}{2} \sum_{i=0}^{i_{\max}-1} \left\{ \left[(r_{i+1})^2 - (r_i)^2 \right] \left[\frac{(\alpha_{H_2} \rho V)_{i+1} + (\alpha_{H_2} \rho V)_i}{2} \right] \right\}$$

REFERENCES

1. Beach, H. L., Jr.: Supersonic Mixing and Combustion of a Hydrogen Jet in a Coaxial High-Temperature Test Gas. AIAA Paper No. 72-1179, Nov.-Dec. 1972.
2. Billig, F. S., Orth, R. C., and Funk, J. A.: Direct-Connect Tests of a Hydrogen-Fueled Supersonic Combustor. NASA CR 1904, 1971.
3. Engineering Staff: Hypersonic Research Engine Project - Phase II. Combustor Program. Final Technical Data Report, Doc. No. Ap-70-6054 (Contract NAS 1-6666), AiResearch Manufacturing Co., Mar. 23, 1970. (Available as NASA CR-66932.)
4. Burrows, M. C.; and Kurkov, A. P.: Supersonic Combustion of Hydrogen in a Vitiated Air Stream Using Stepped-Wall Injection: AIAA paper No. 71-721, June 1971.
5. Cohen, Leonard S.; and Guile, Roy N.: Investigation of the Mixing and Combustion of Turbulent, Compressible Free Jets. NASA CR-1473, 1969.
6. Davis, R. E.: An Experimental Investigation of the Supersonic Combustion of Vitiated Air-H₂ Mixtures. AEDC-TR-70-60, May 1970.
7. Anon.: Engineering Analyses and Design Calculation of NASA Langley Research Center Hydrogen-Air-Vitiated Heater With Oxygen Replenishment. Tech. Memo. No. 173, Gen. Appl. Sci. Labs., Inc., 1974. (Available as NASA CR-132381.)
8. Harrje, David T.; and Reardon, Frederick H., eds.: Liquid Propellant Rocket Combustion Instability. NASA SP-194, 1972.
9. Heidmann, Marcus F.; Sokolowski, David E.; and Kiehl, Lawrence A.: Study of Chugging Instability With Liquid-Oxygen and Gaseous-Hydrogen Combustors. NASA TN D-4005, 1966.
10. Anon.: Van Nostrand's Scientific Encyclopedia. Third ed., D. Van Nostrand, Co., Inc., c.1958.
11. Wood, Don J.; and Dorsch, Robert G.: Effect of Propellant-Feed-System Coupling and Hydraulic Parameters on Analysis of Chugging. NASA TN D-3896, 1967.
12. Drell, Isadore L.; and Belles, Frank E.: Survey of Hydrogen Combustion Properties. NACA Rep. 1383, 1958. (Supersedes NACA RM E57D24.)
13. Kreith, F.: Principles of Heat Transfer. Int. Textbook Co. (Scranton, Pa.), c.1958.
14. Schlichting, Hermann (J. Kestin, transl.): Boundary-Layer Theory. Sixth ed., McGraw-Hill Book Co., Inc., 1968.

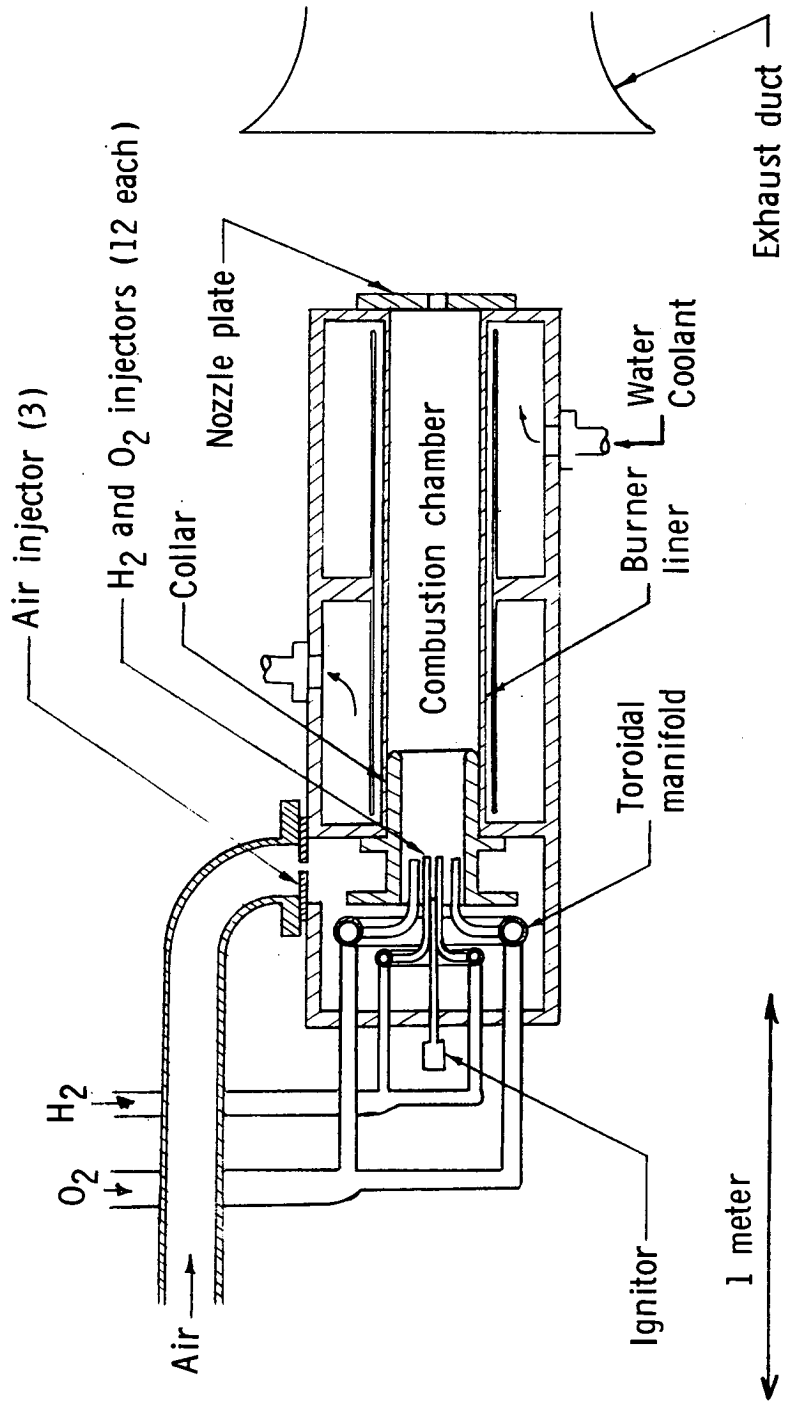


Figure 1.- Hydrogen burner.

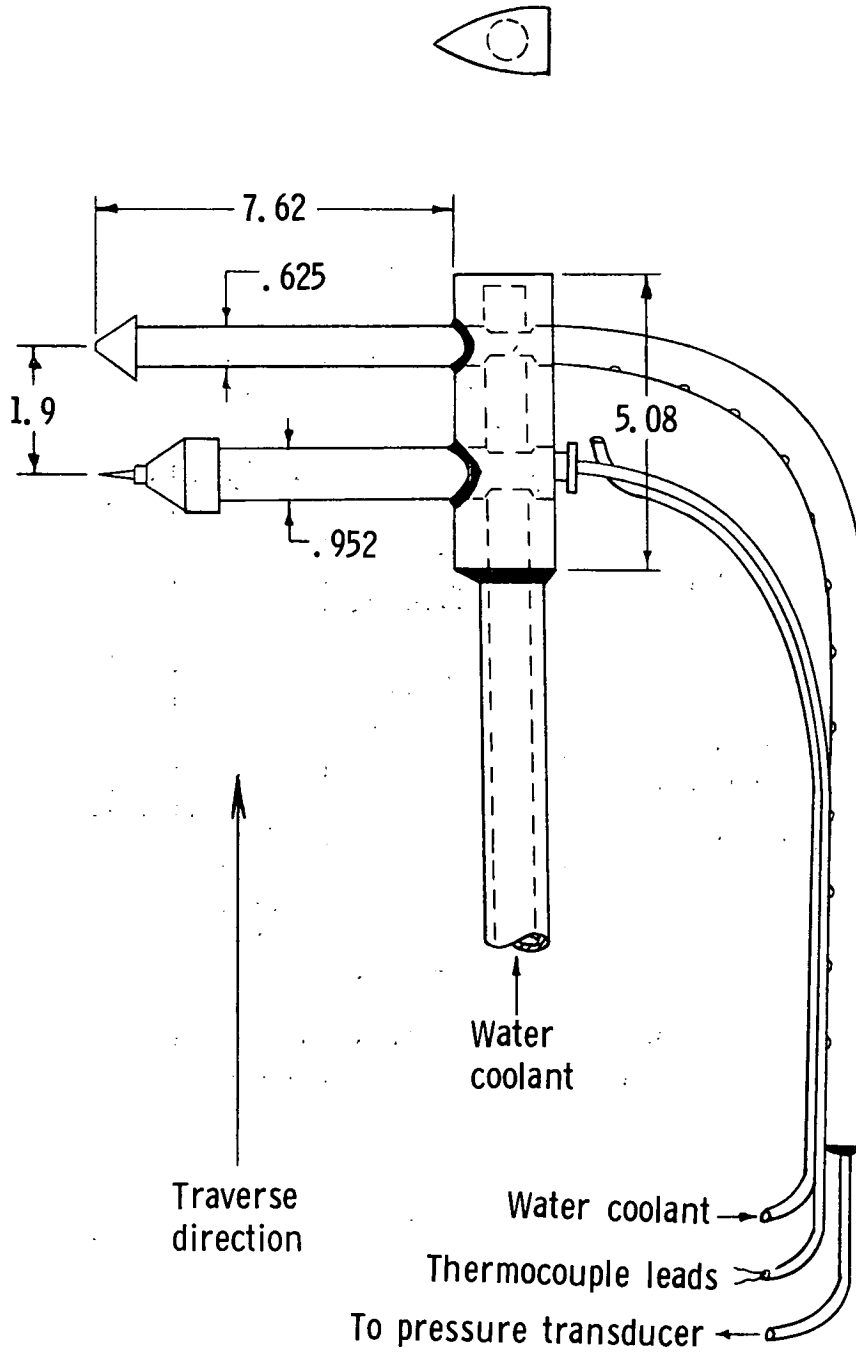


Figure 2.- Traverse probe. Dimensions are in centimeters.

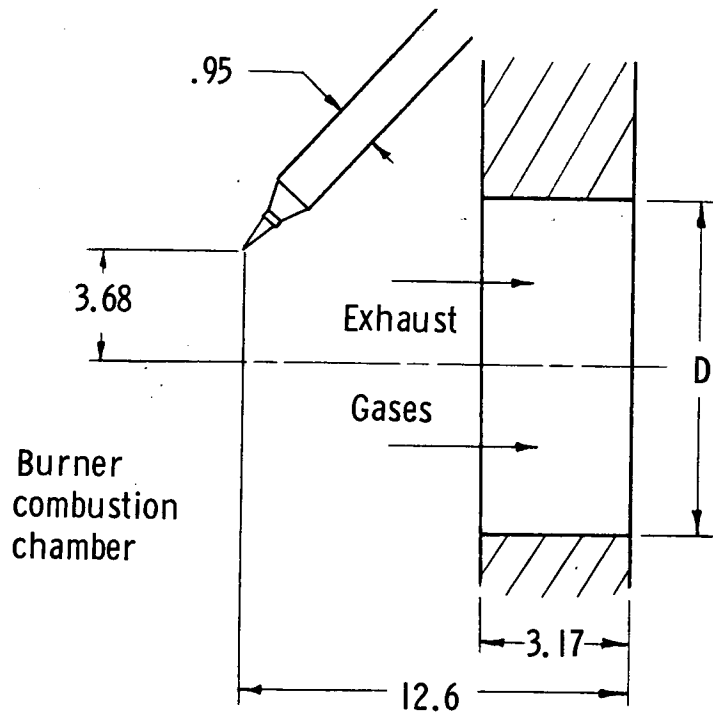


Figure 3.- Burner thermocouple probe.
Dimensions are in centimeters.

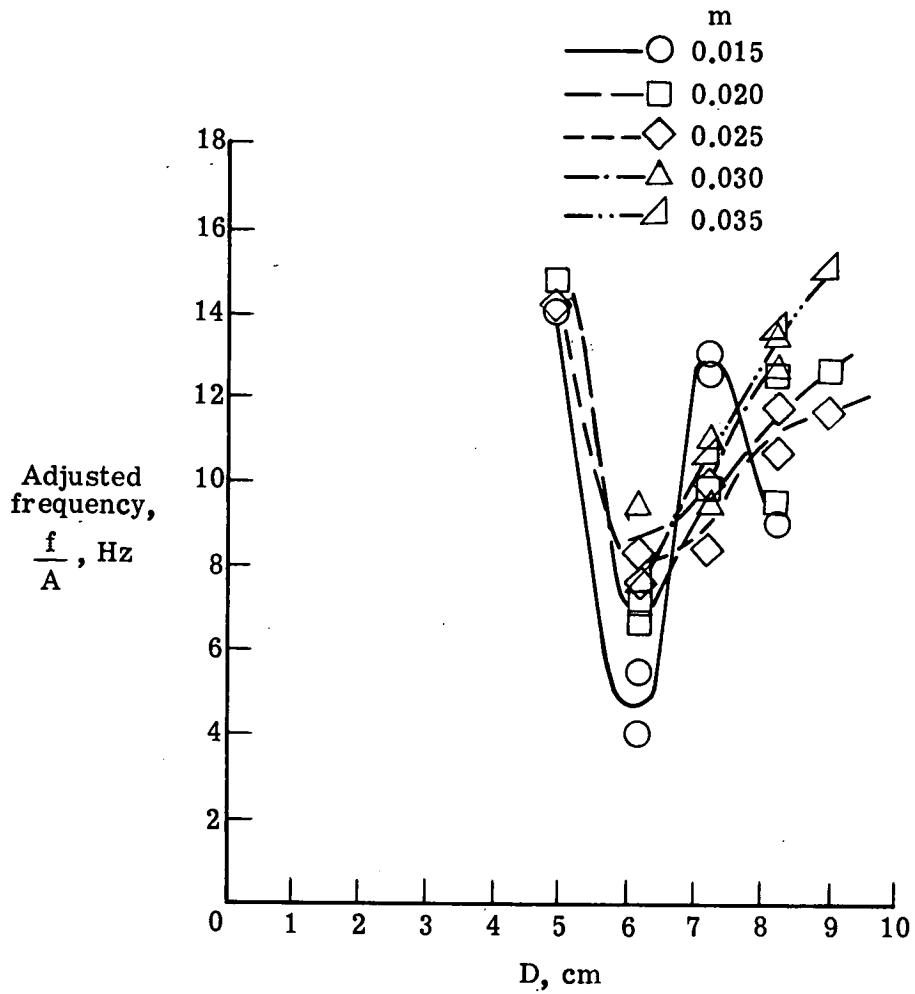


Figure 4.- Burner system frequency as a function of nozzle throat diameter.

$$A = \sqrt{\frac{\left(\frac{\gamma T}{M}\right)_m}{\left(\frac{\gamma T}{M}\right)_{m=0.015}}}$$

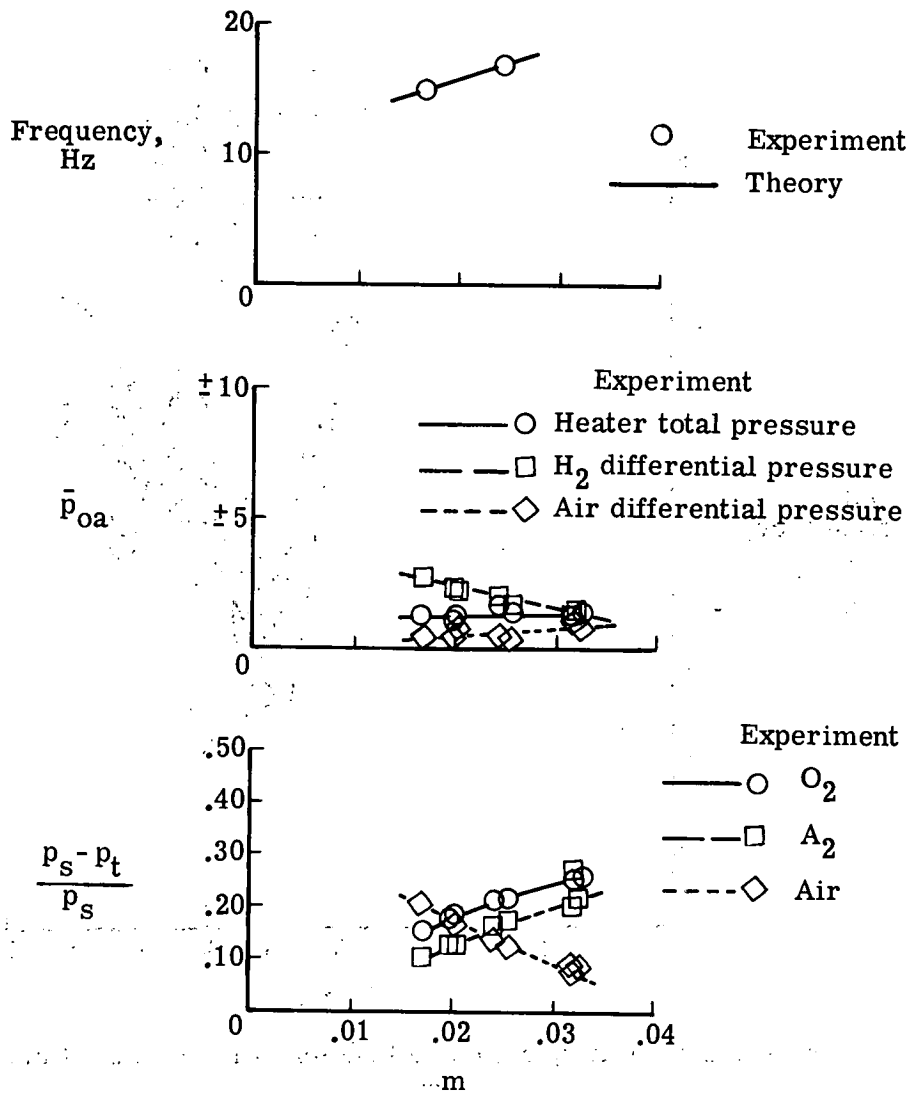


Figure 5.- Pressure oscillation parameters as a function of mixture ratio for test 46 ($D = 4.83$ cm) at $p_t = 0.69$ MN/m². Injector diameters, cm: H₂, 0.259; O₂, 0.450; and air, 1.59.

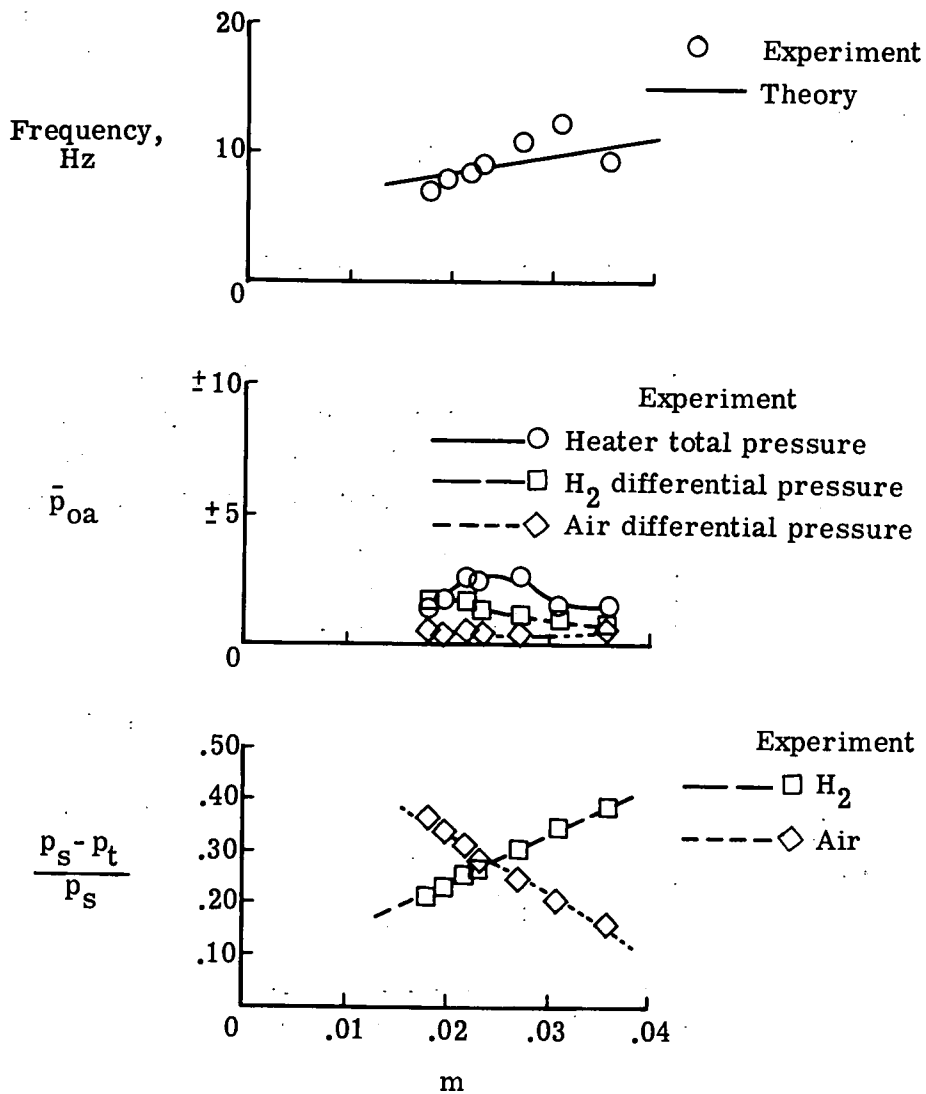


Figure 6.- Pressure oscillation parameters as a function of mixture ratio for test 49 ($D = 6.04$ cm) at $p_t = 0.69$ MN/m². Injector diameter, cm: H_2 , 0.259; O_2 , 0.450; and air, 1.59.

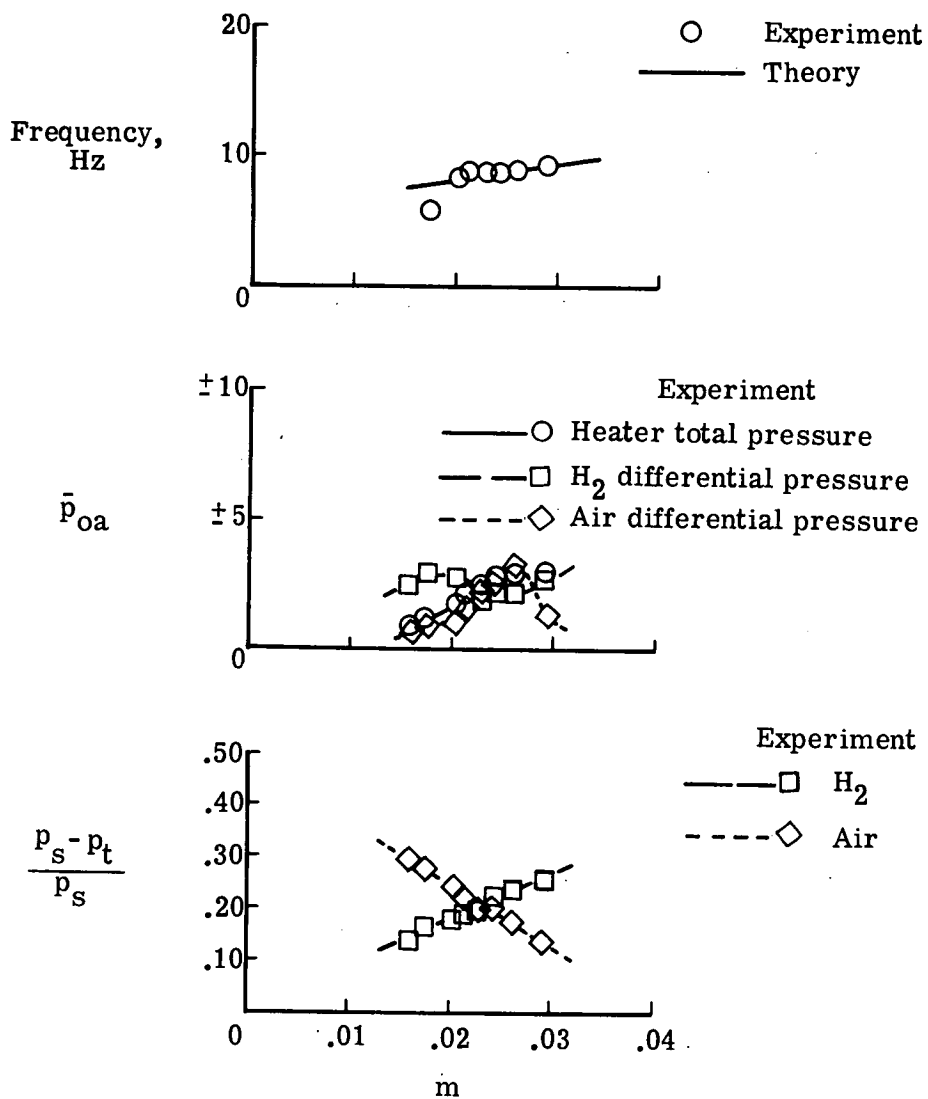


Figure 7.- Pressure oscillation parameters as a function of mixture ratio test 50 ($D = 6.04$ cm) at $p_t = 0.69$ MN/m². Injector diameter, cm: H₂, 0.307; O₂, 0.531; and air, 1.83.

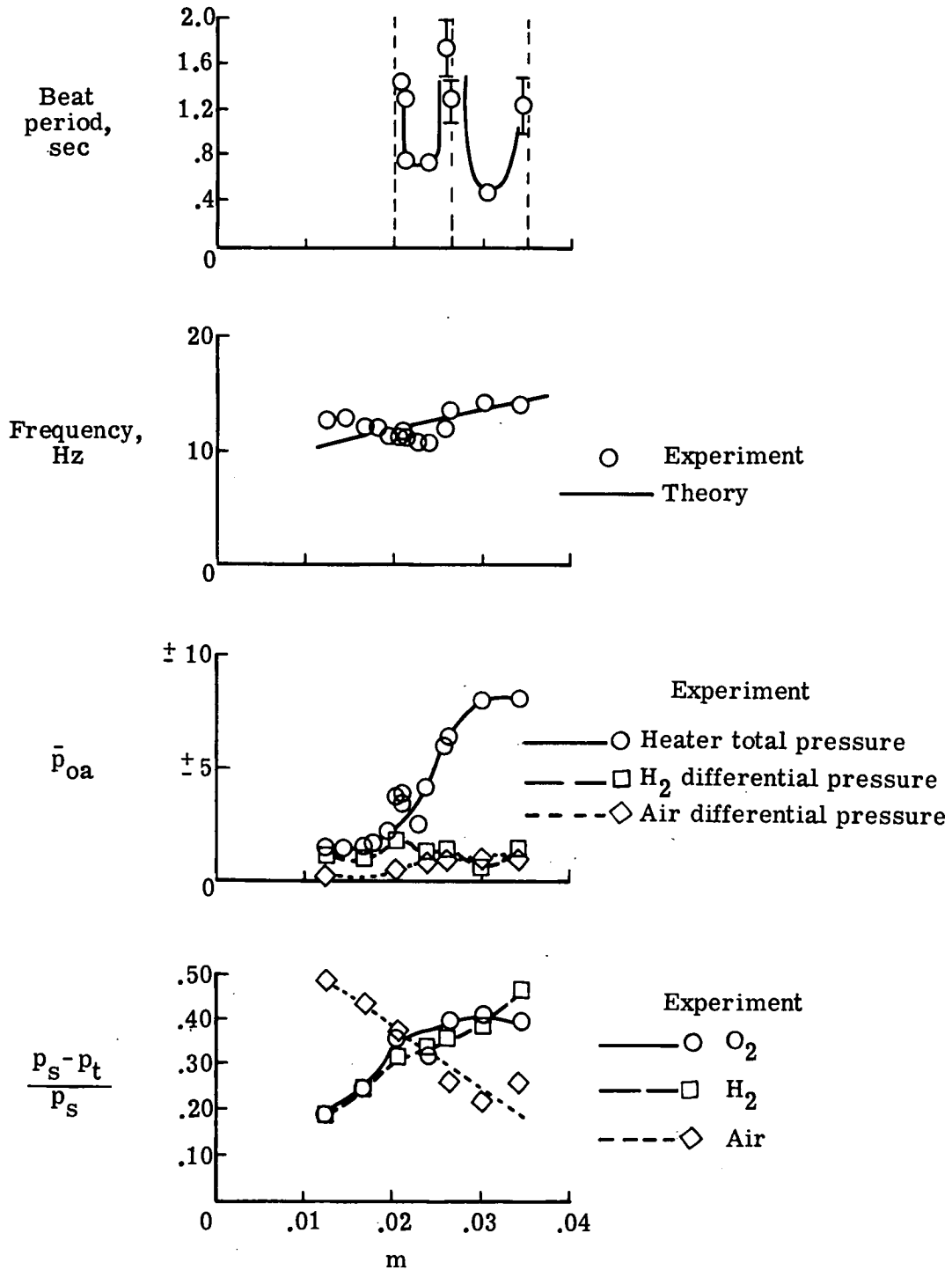


Figure 8.- Pressure oscillation parameters as a function of mixture ratio for test 52 ($D = 7.12$ cm) at $p_t = 0.69$ MN/m². Injector diameter, cm: H_2 , 0.307; O_2 , 0.531; and air, 1.83.

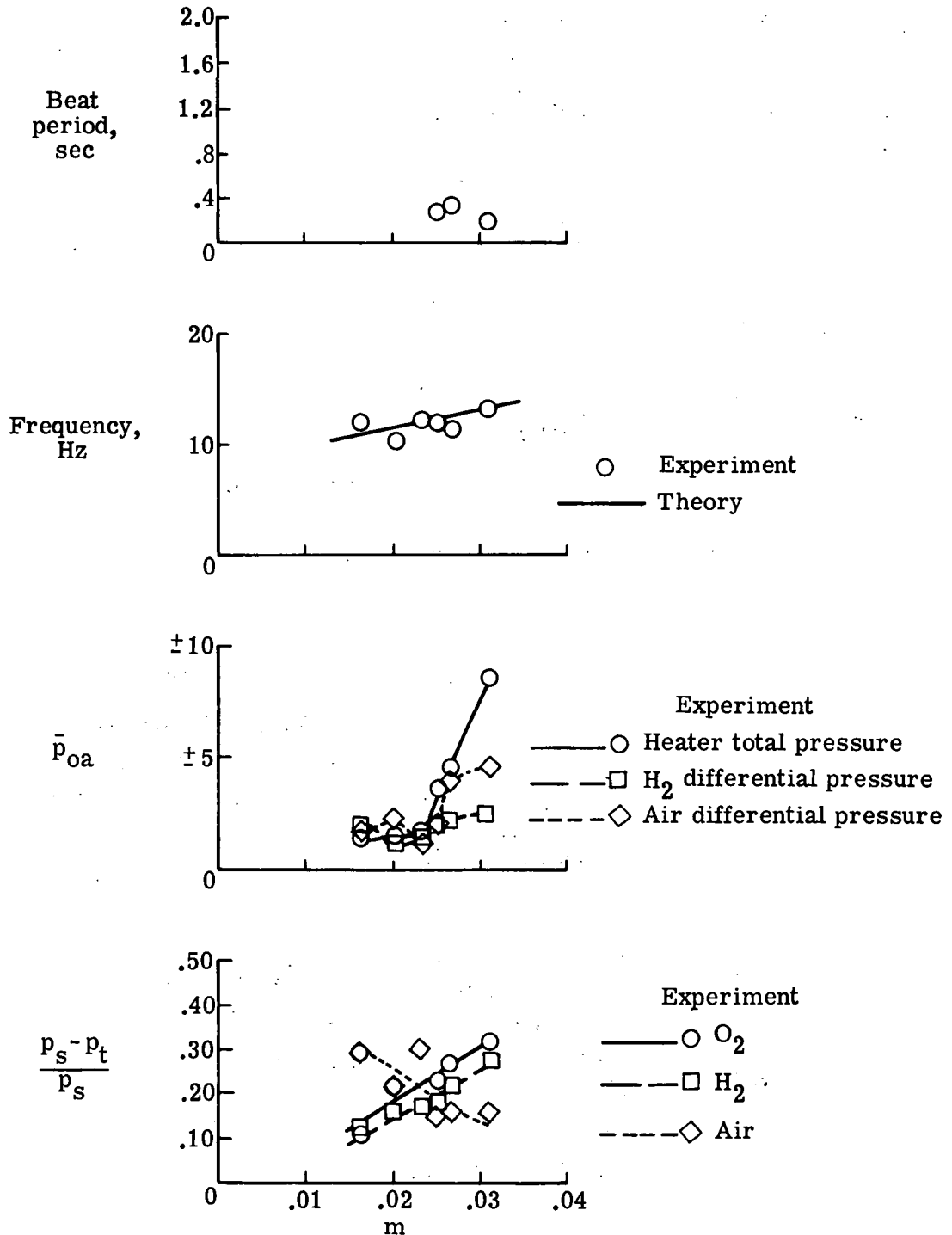


Figure 9.- Pressure oscillation parameters as a function of mixture ratio for test 53 ($D = 7.12$ cm) at $p_t = 0.69$ MN/m². Injector diameter, cm: H_2 , 0.396; O_2 , 0.635; and air, 2.19.

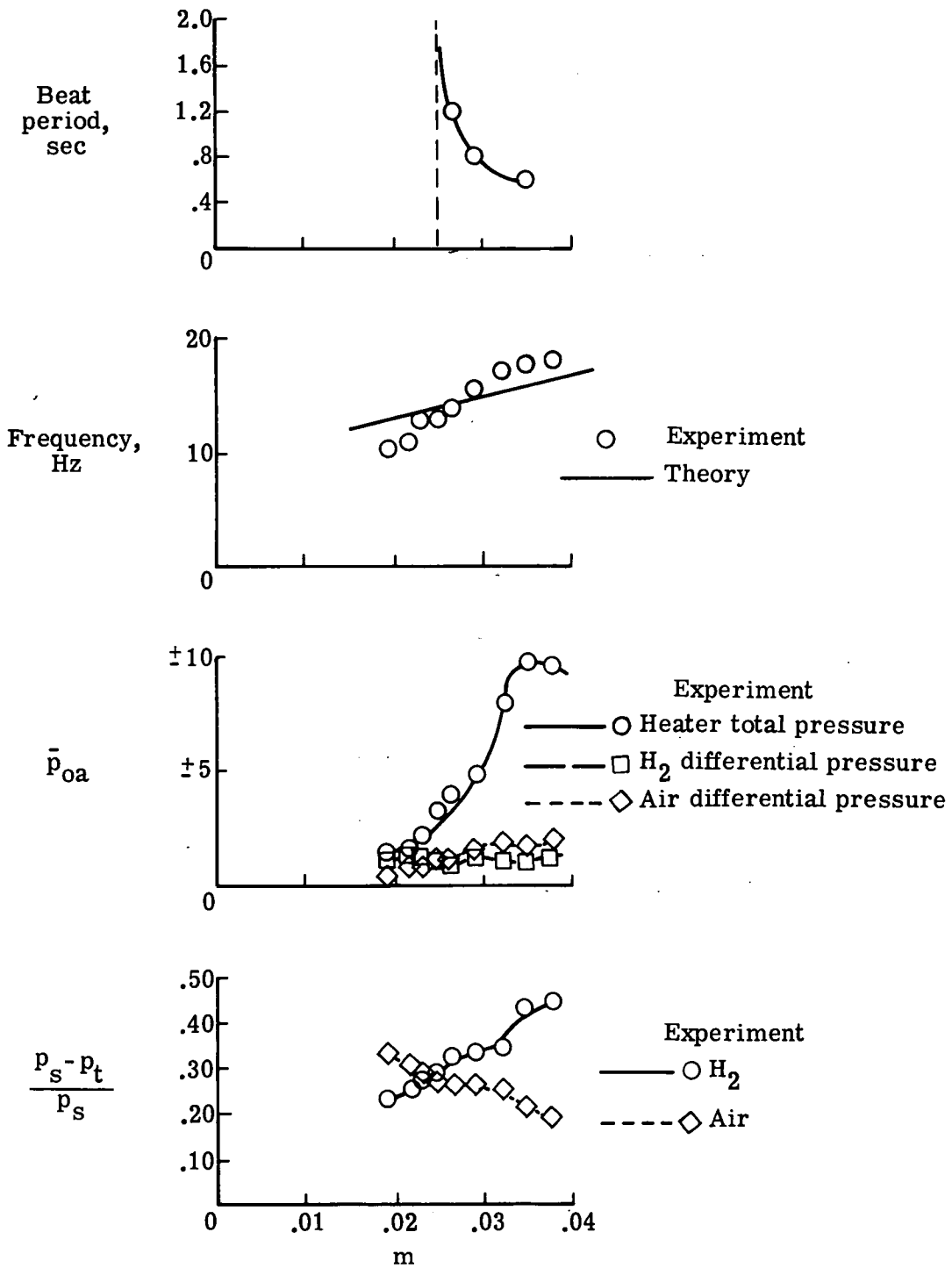


Figure 10.- Pressure oscillation parameters as a function of mixture ratio for test 54 ($D = 8.13$ cm) at $p_t = 0.69$ MN/m². Injector diameter, cm: H₂, 0.396; O₂, 0.635; and air, 2.19.

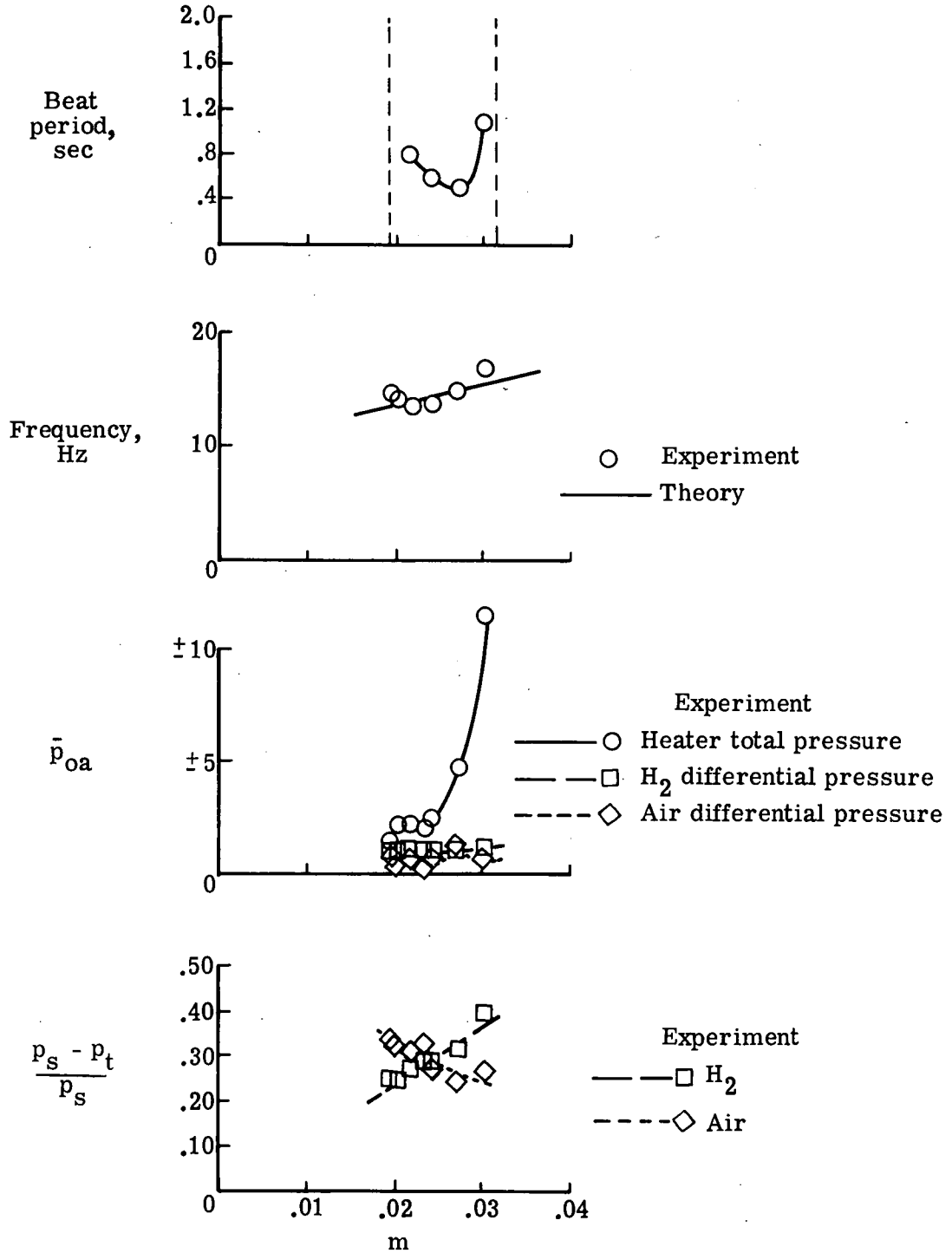


Figure 11.- Pressure oscillation parameters as a function of mixture ratio for test 55 ($D = 8.13$ cm) at $p_t = 0.69$ MN/m². Injector diameter, cm: H_2 , 0.396; O_2 , 0.635; and air, 2.34.

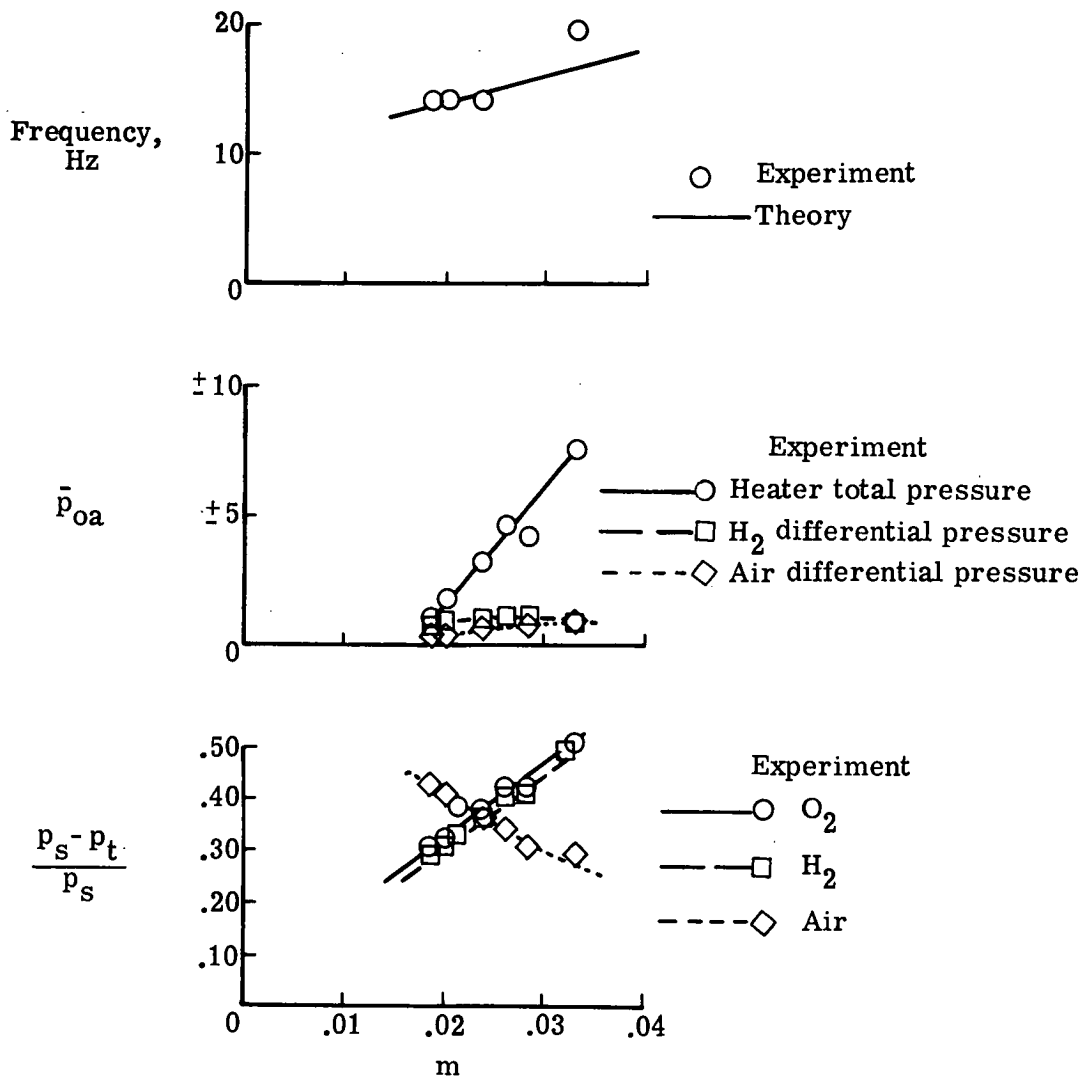


Figure 12.- Pressure oscillation parameters as a function of mixture ratio for test 55 ($D = 8.89$ cm) at $p_t = 0.69$ MN/m². Injector diameter, cm: H_2 , 0.396; O_2 , 0.635; and air, 2.34.

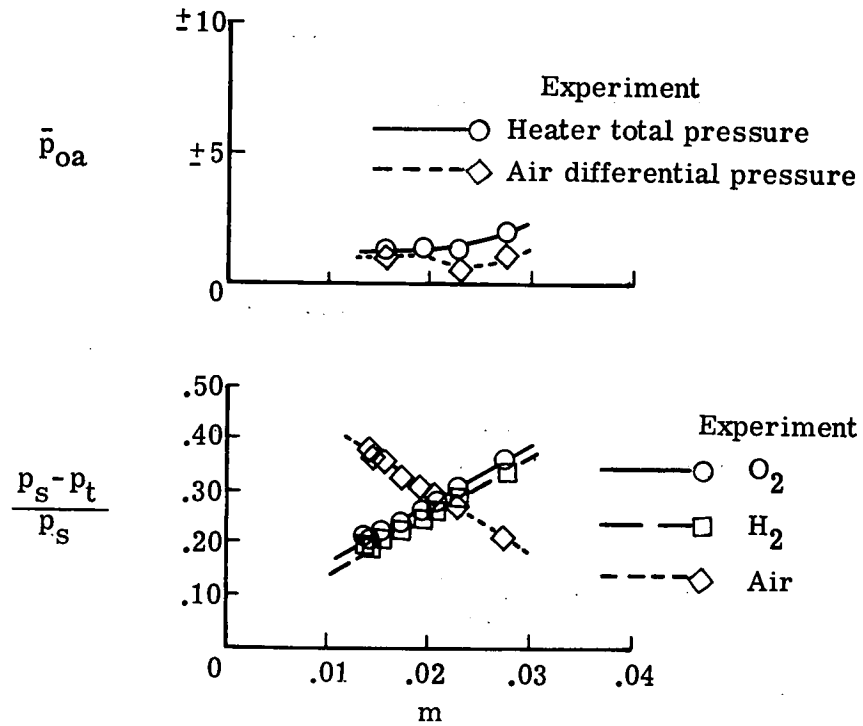


Figure 13.- Pressure oscillation parameters as a function of mixture ratio for test 72 ($D = 8.89$ cm) of $p_t = 0.69$ MN/m². Injector diameter, cm: H_2 , 0.470; O_2 , 0.742; and air, 2.79.

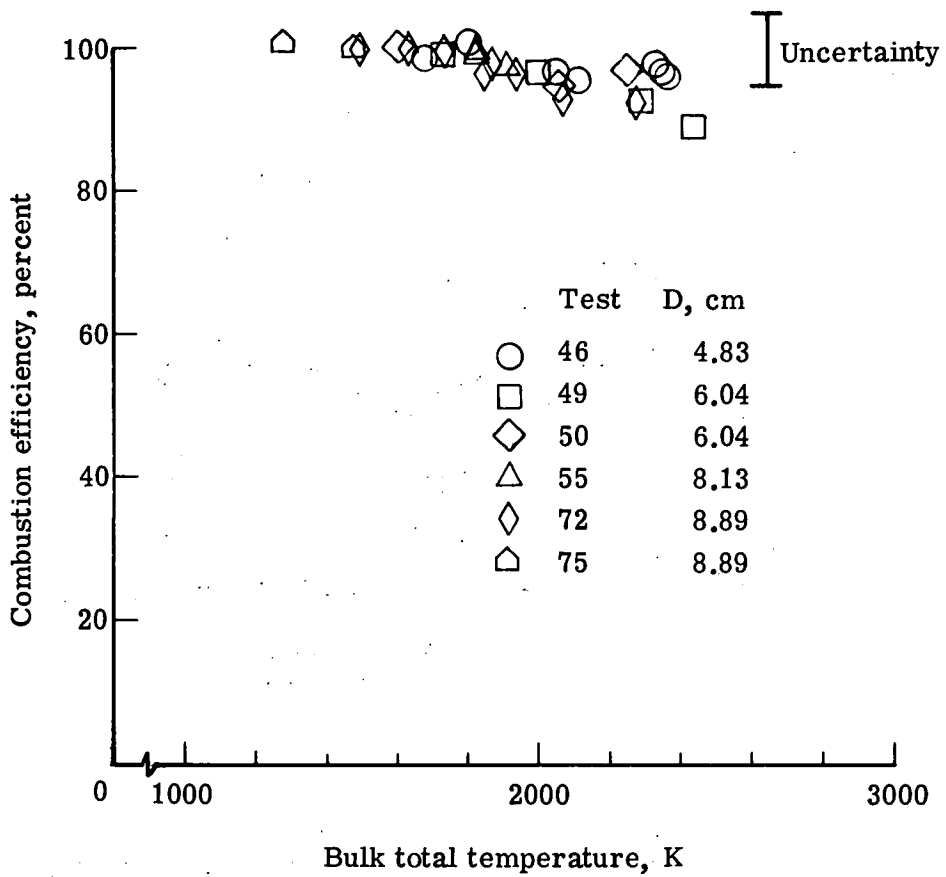


Figure 14.- Combustion efficiency as a function of theoretical bulk total temperature. $C_d = 0.866$.

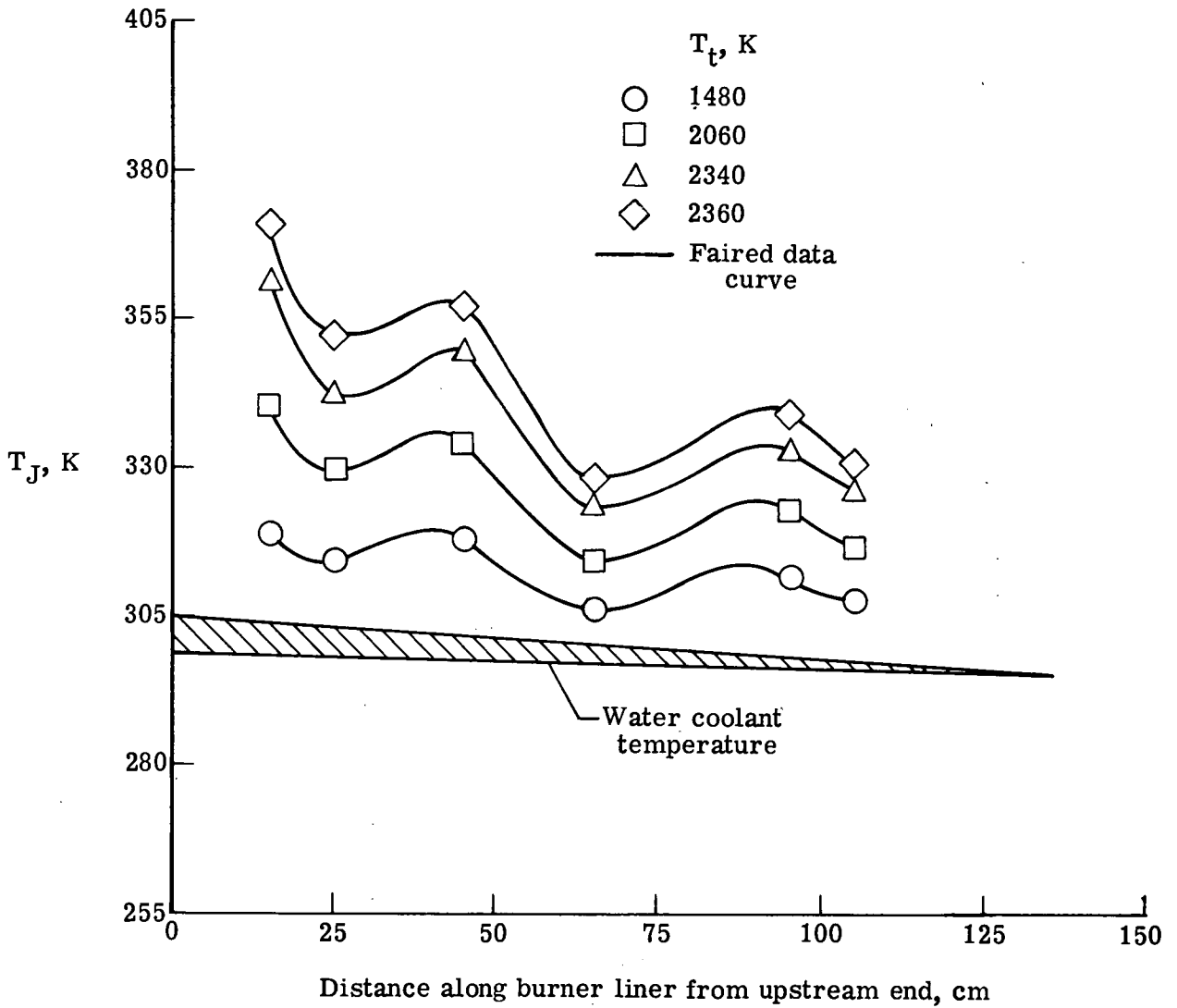


Figure 15.- Burner liner temperature distribution for exhaust port diameter of 4.83 cm. Test 46; $D = 4.83$ cm.

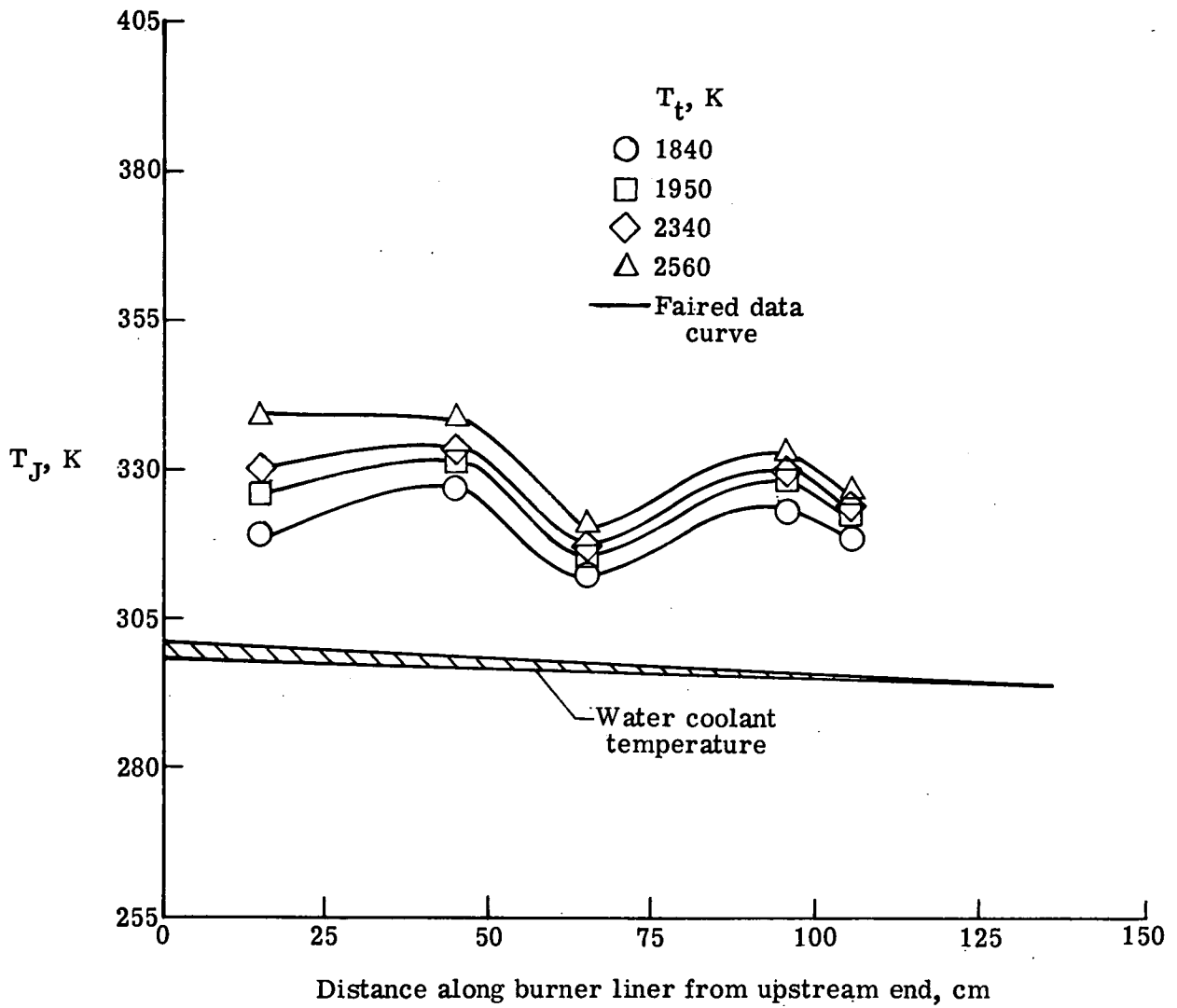


Figure 16.- Burner liner temperature distribution for exhaust port diameter of 8.89 cm. Test 56; $D = 8.89$ cm.

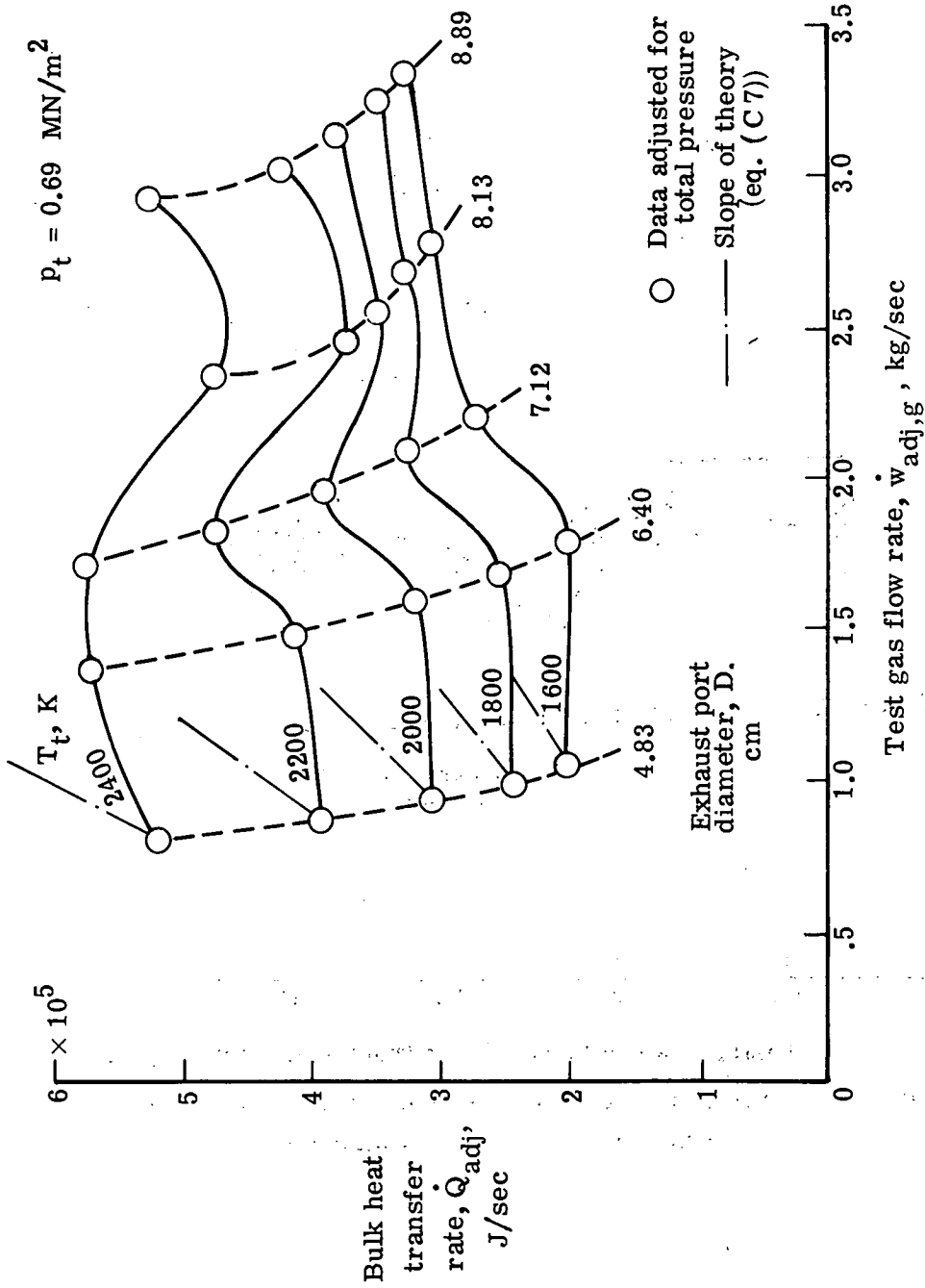


Figure 17.- Measured bulk heat-transfer rate map. $p_t = 0.69 \text{ MN/m}^2$.

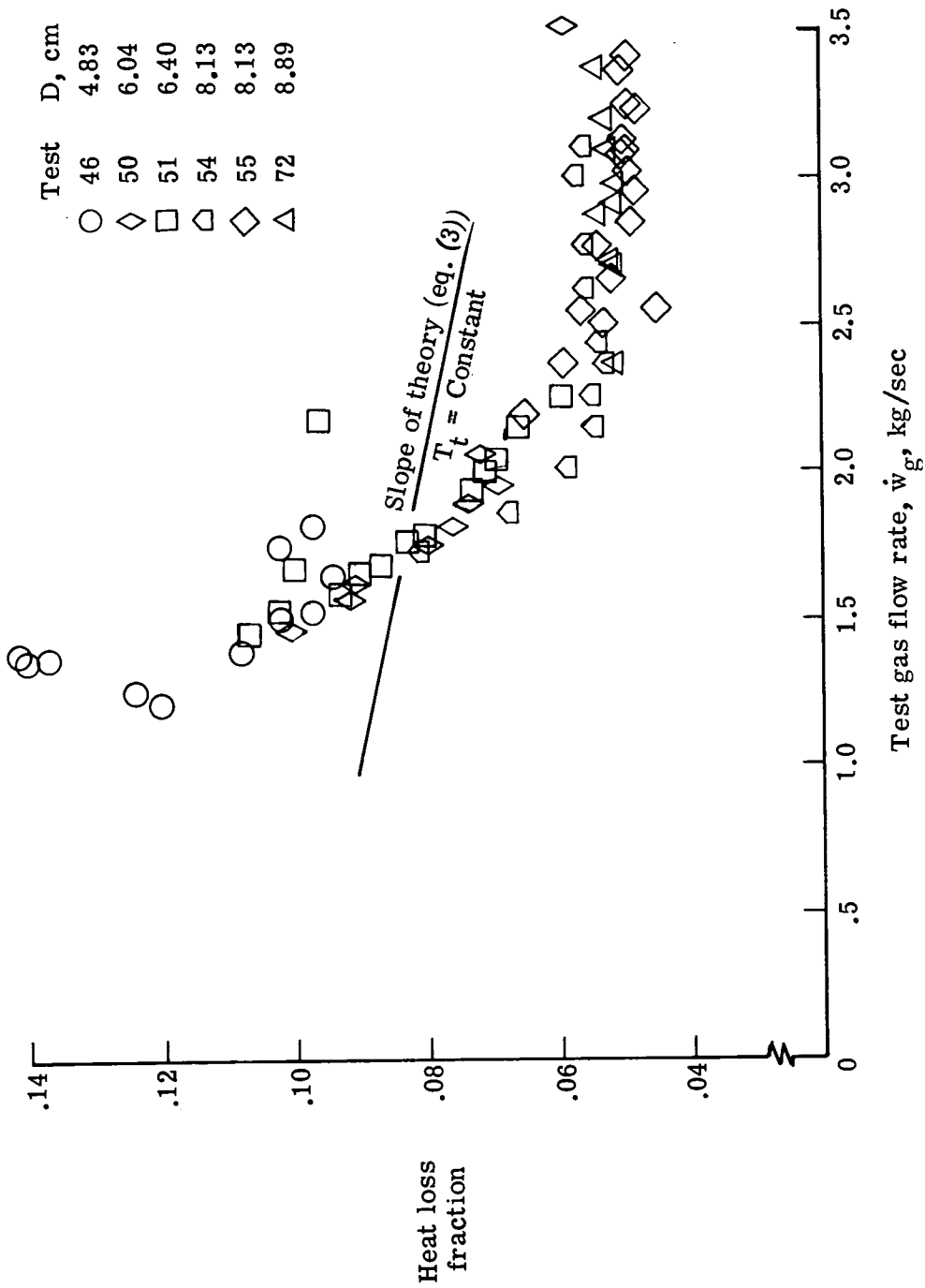


Figure 18.- Variation of heat loss fraction (eq. (C8)) with test gas flow rate.

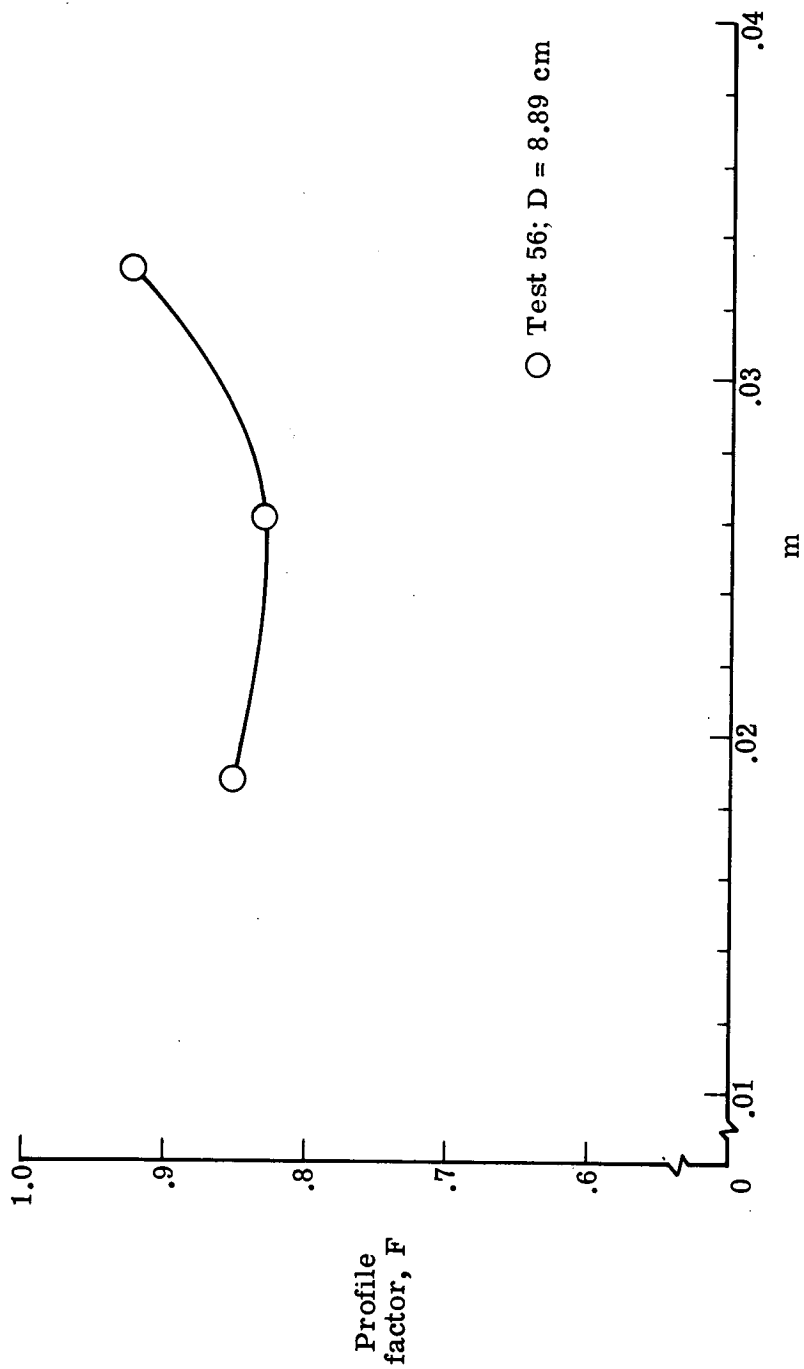


Figure 19.- Variation in temperature profile required to make theoretical hot-gas-side heat transfer equal to that measured.

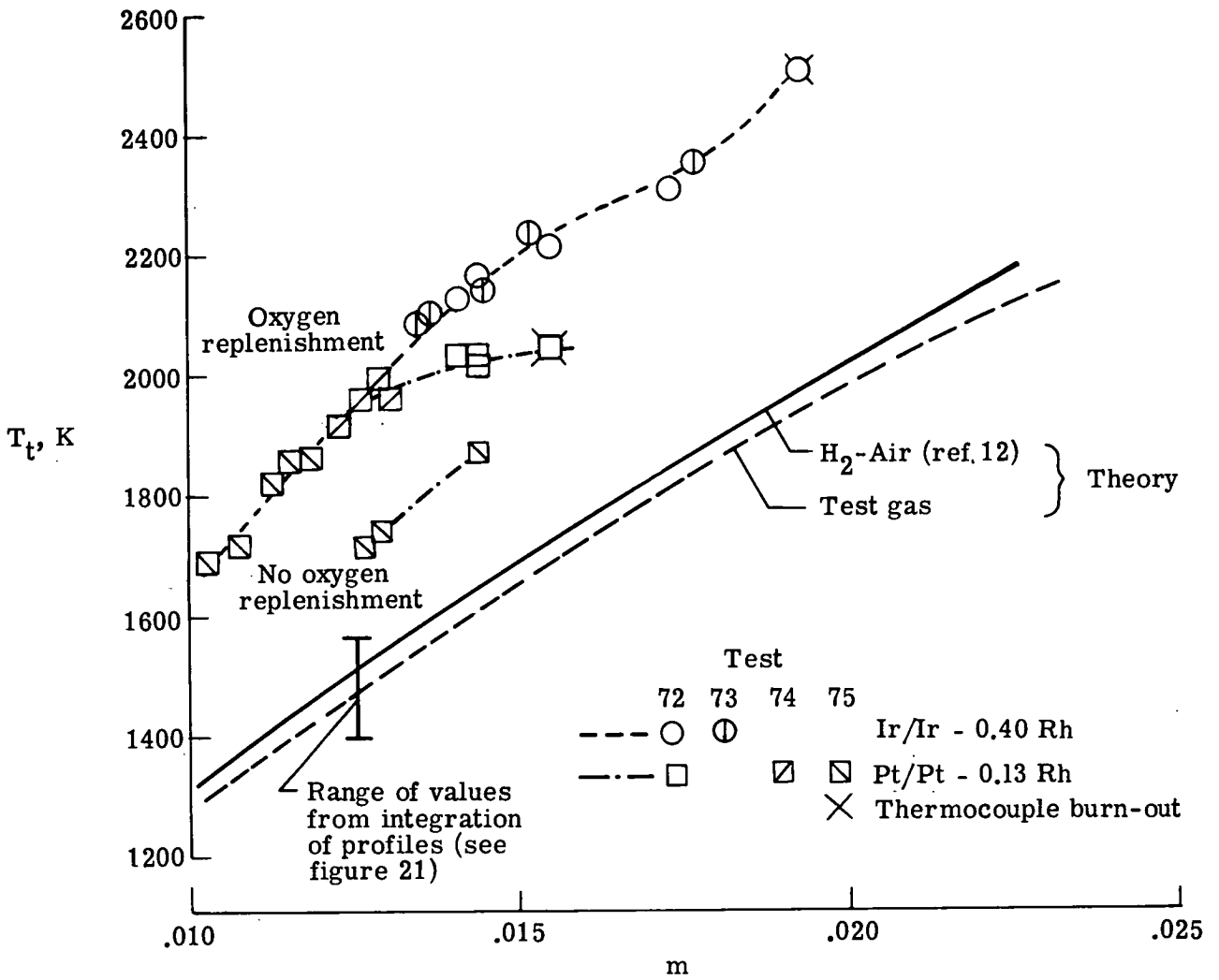


Figure 20.- Thermocouple probe measurements compared with theoretical burner total temperature.

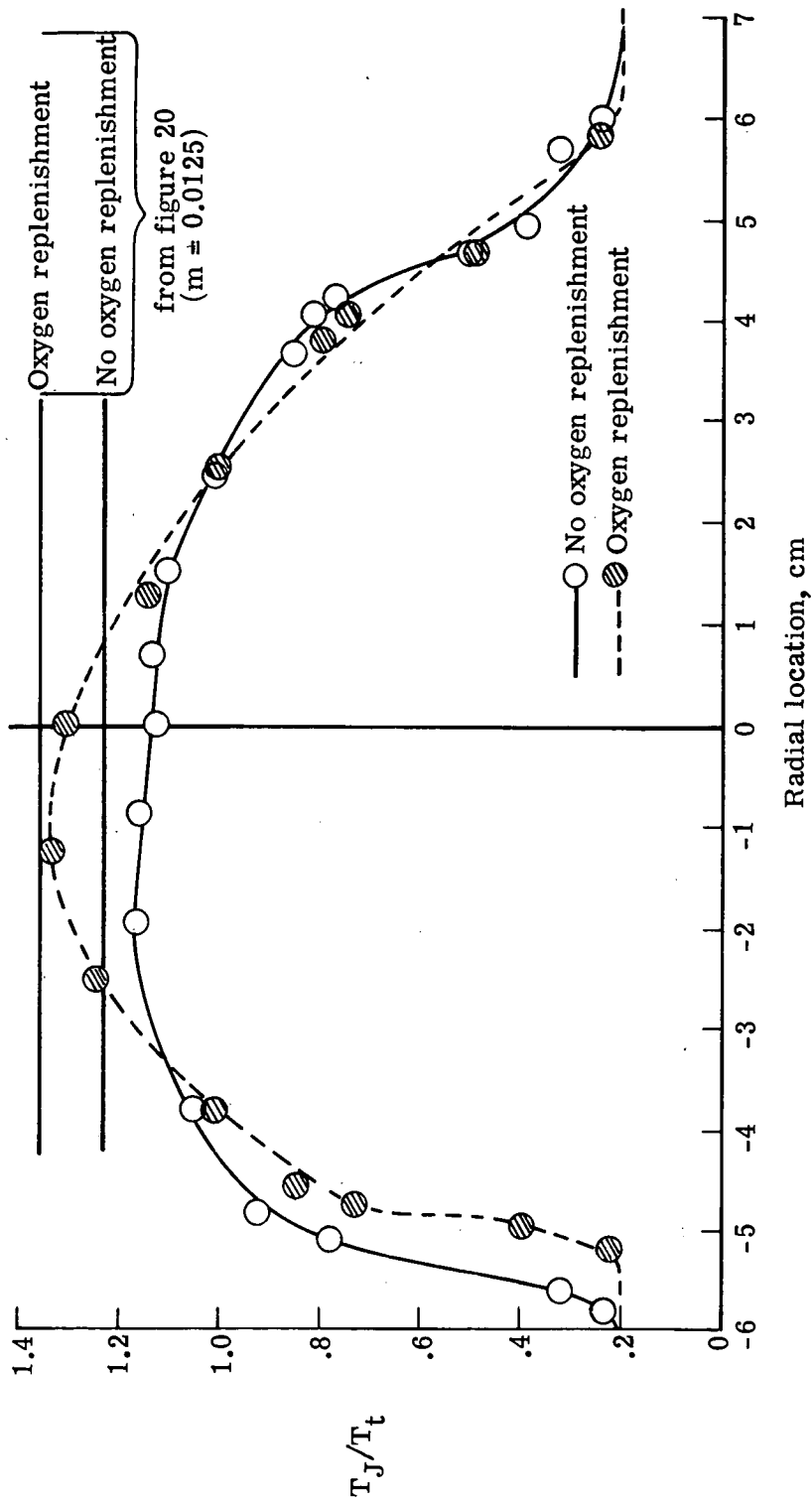


Figure 21.- Exhaust gas radial temperature profiles with and without oxygen replenishment.

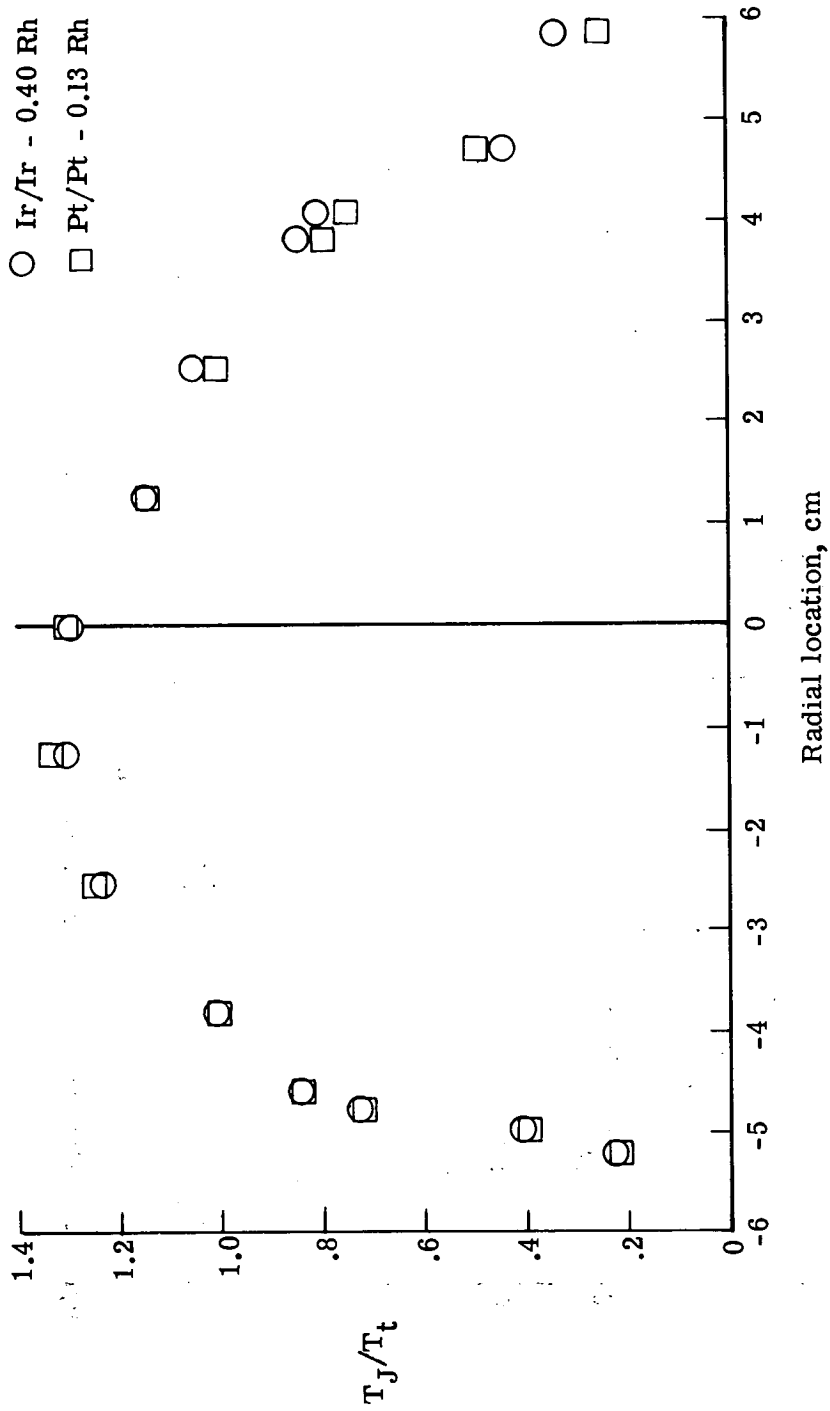


Figure 22.- Comparison of temperature profiles measured with platinum and iridium thermocouples.

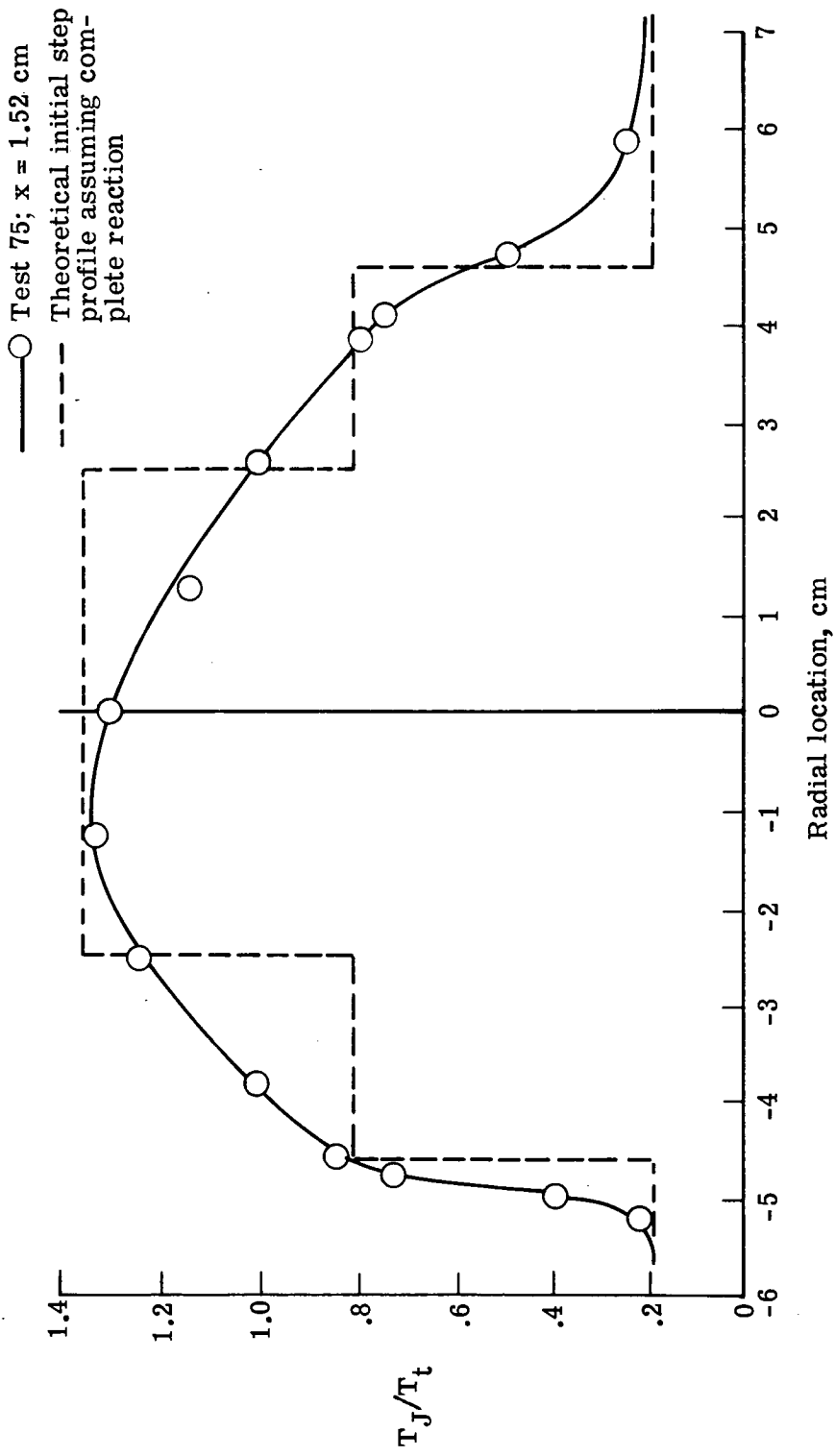


Figure 23.- Comparison of measured temperature profile with the assumed initial profile.

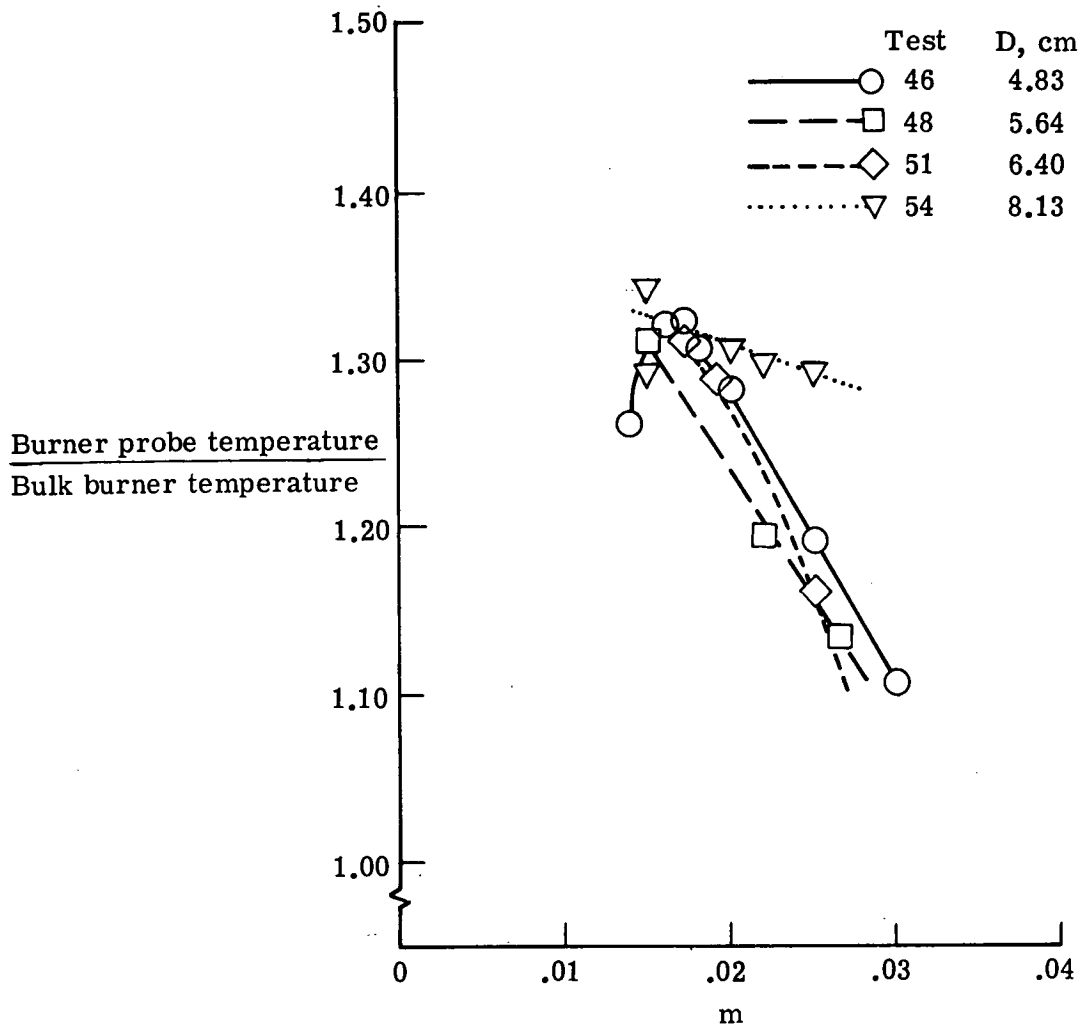


Figure 24.- Variation of degree of temperature profile with burner mixture ratio.

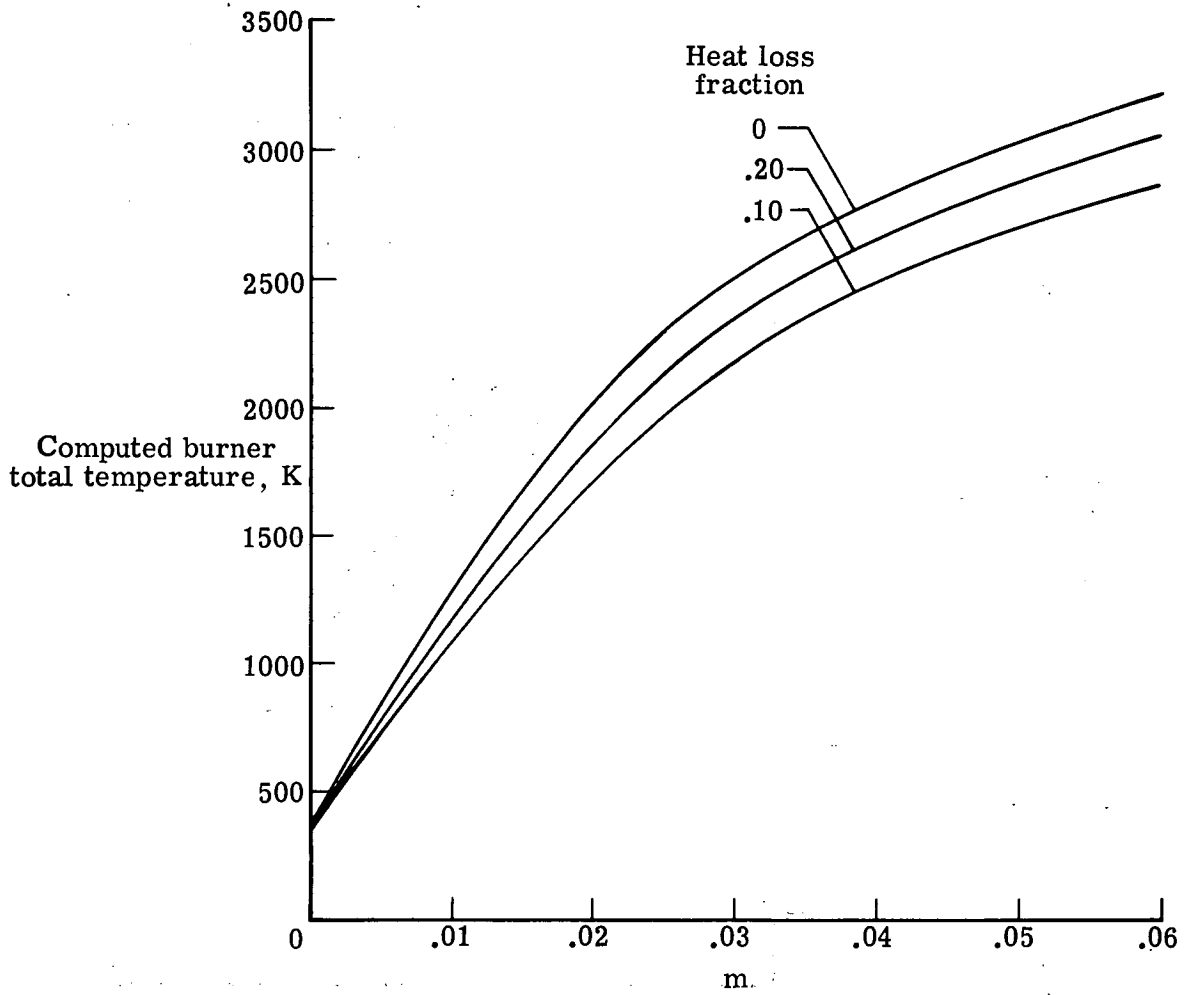


Figure 25.- Burner total temperature as a function of mixture ratio.
Complete combustion assumed.

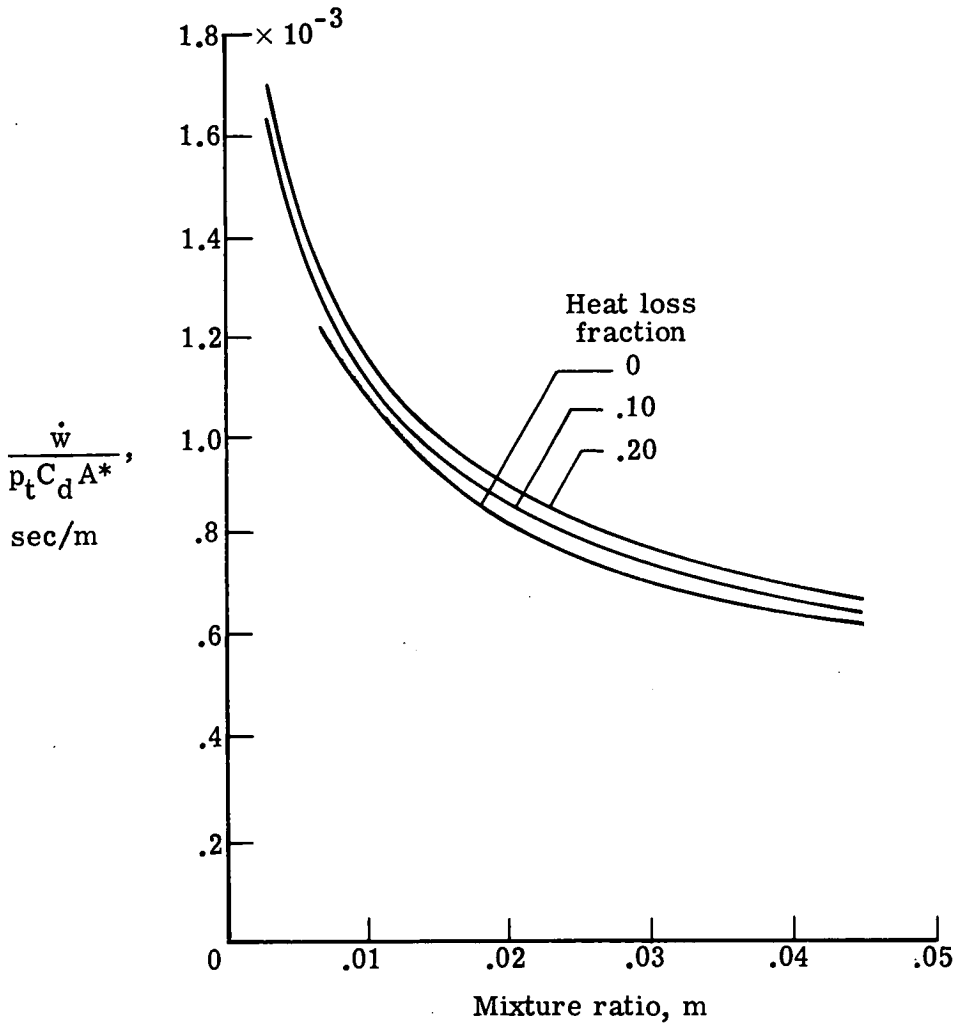


Figure 26.- Burner mass flow parameter as a function of mixture ratio. Oxygen replenishment and complete combustion assumed.

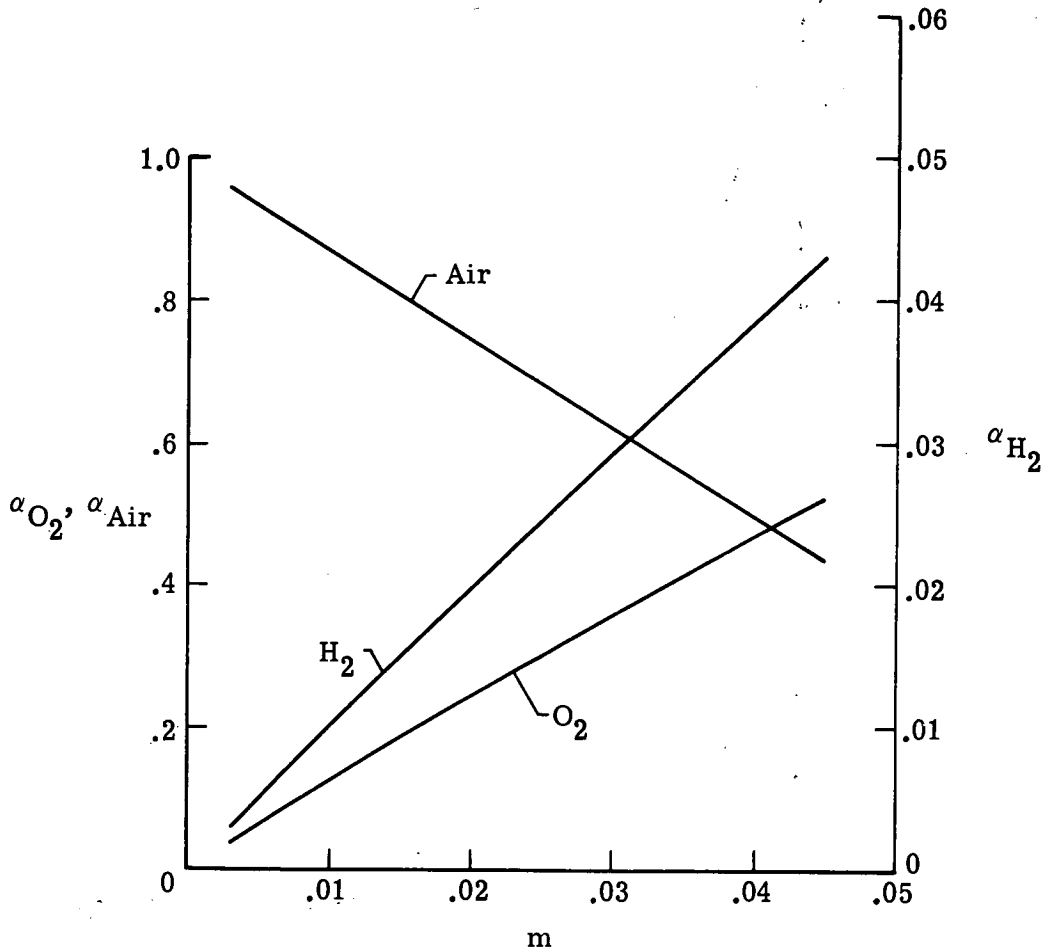


Figure 27.- Initial gas makeup as a function of mixture ratio. Oxygen replenishment and complete combustion assumed.

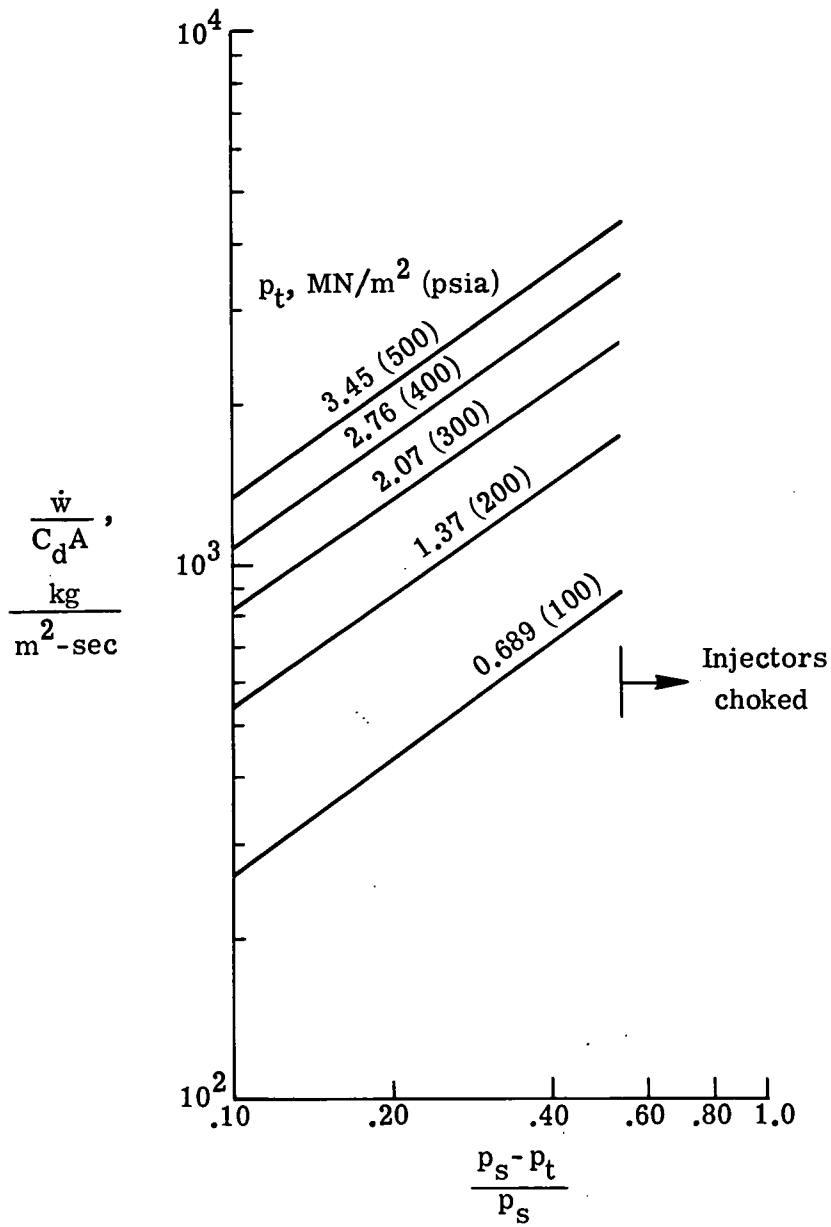


Figure 28.- Hydrogen mass flow as a function of injector pressure drop.

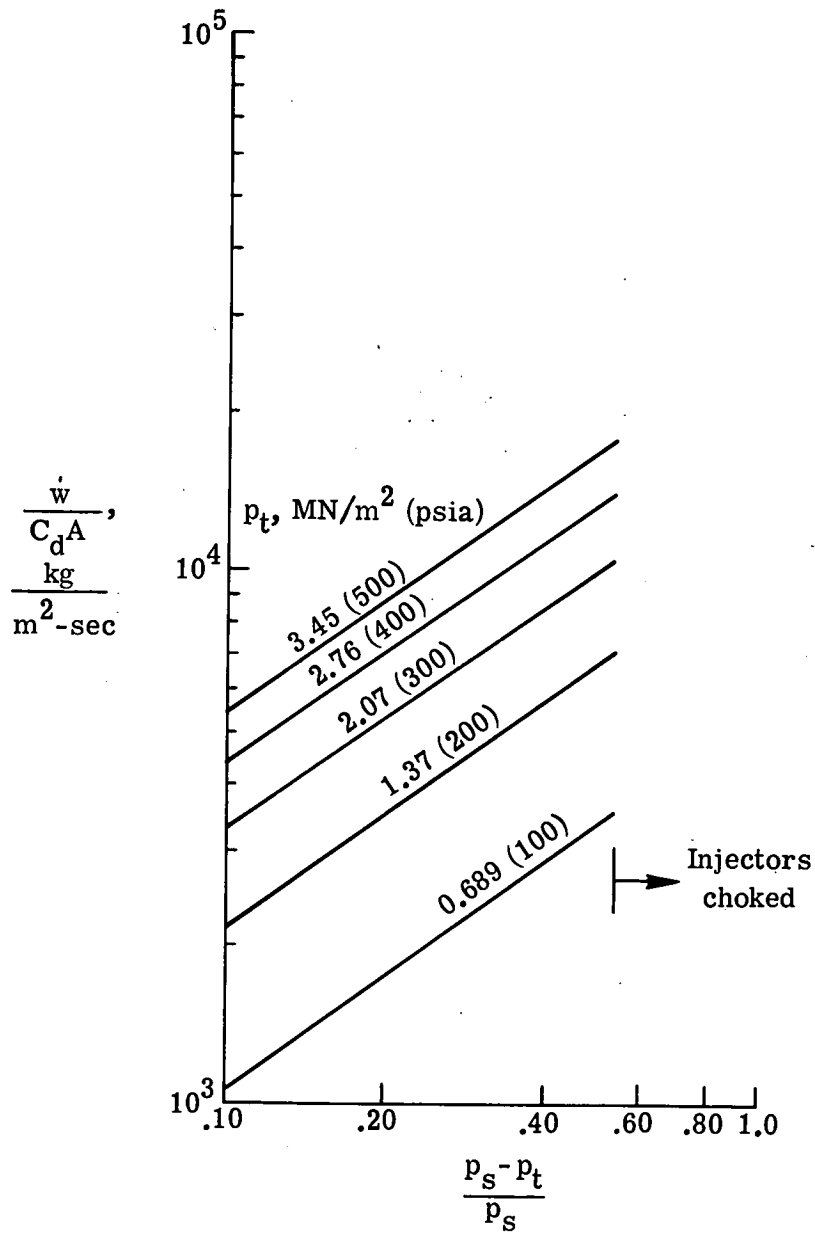


Figure 29.- Oxygen mass flow as a function of injector pressure drop.

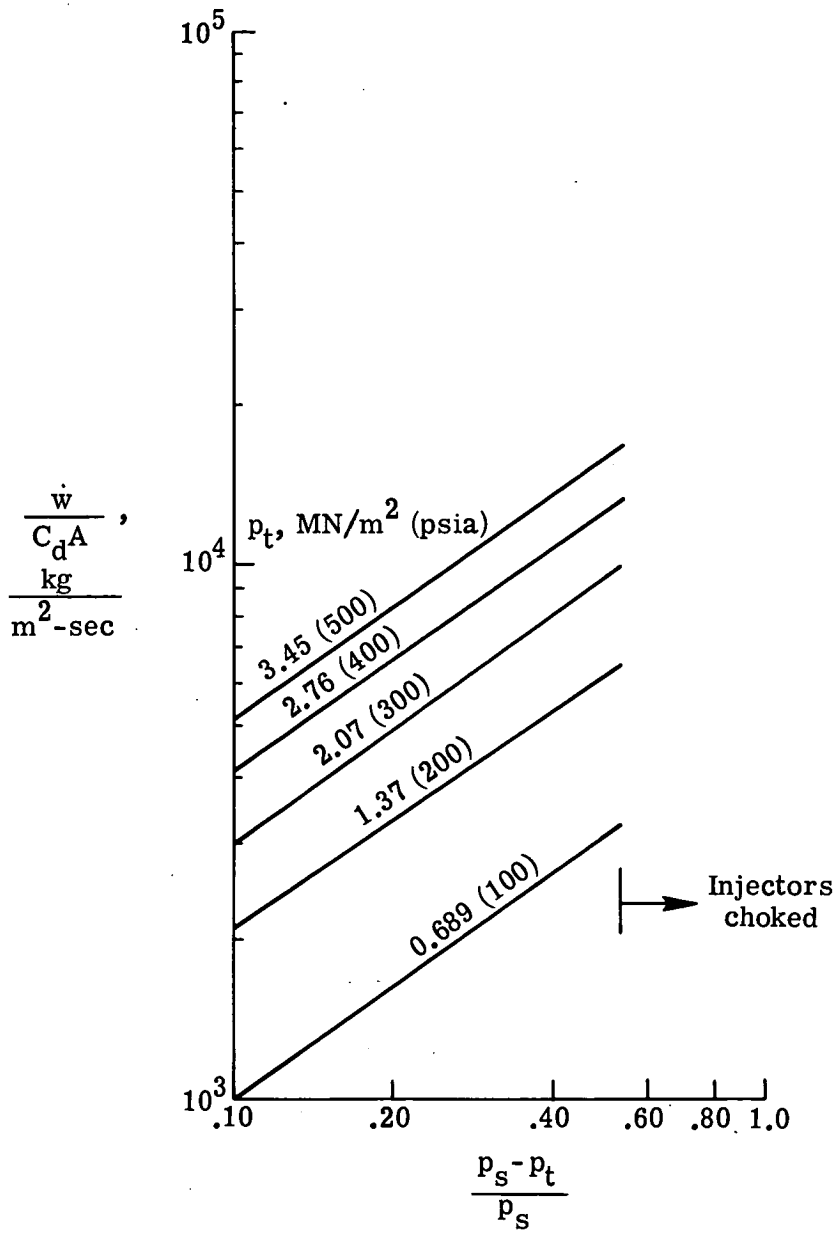


Figure 30.- Air mass flow as a function of injector pressure drop.

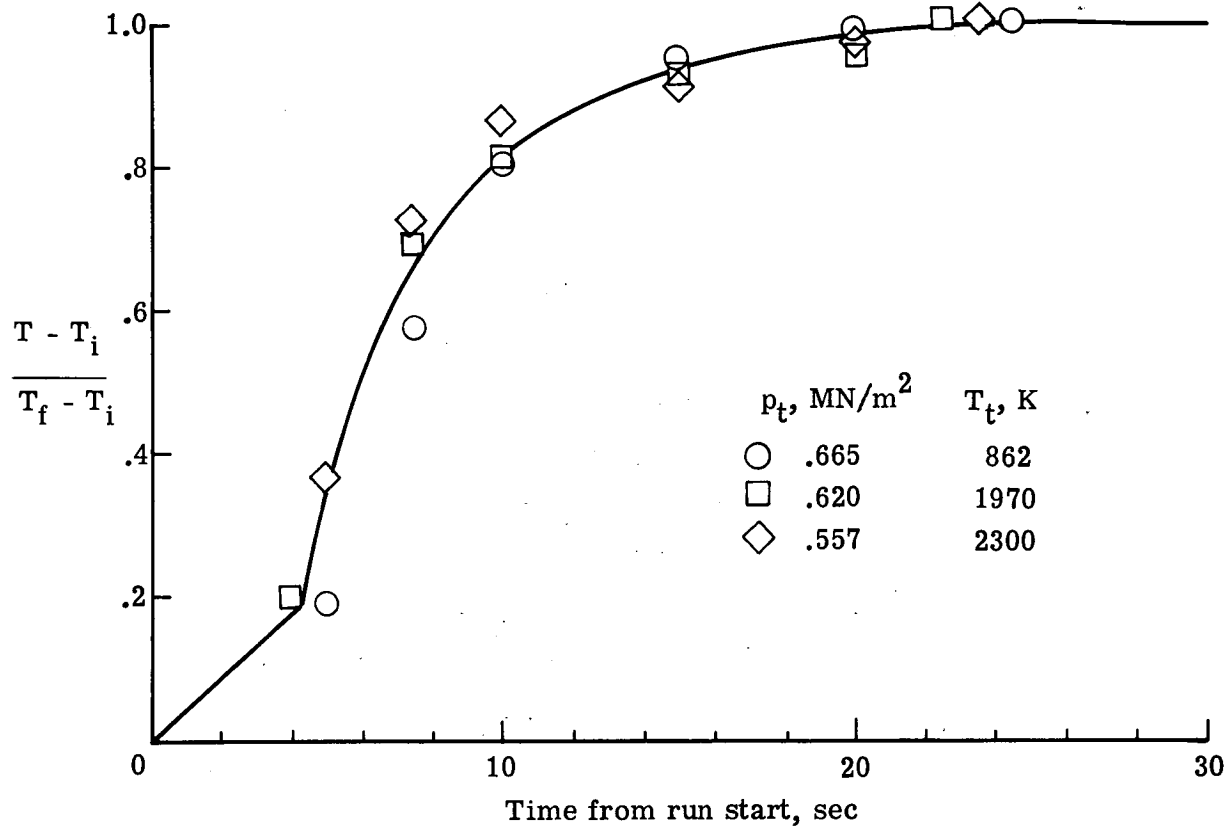


Figure 31.- Time history of cooling water temperature. Test 72.

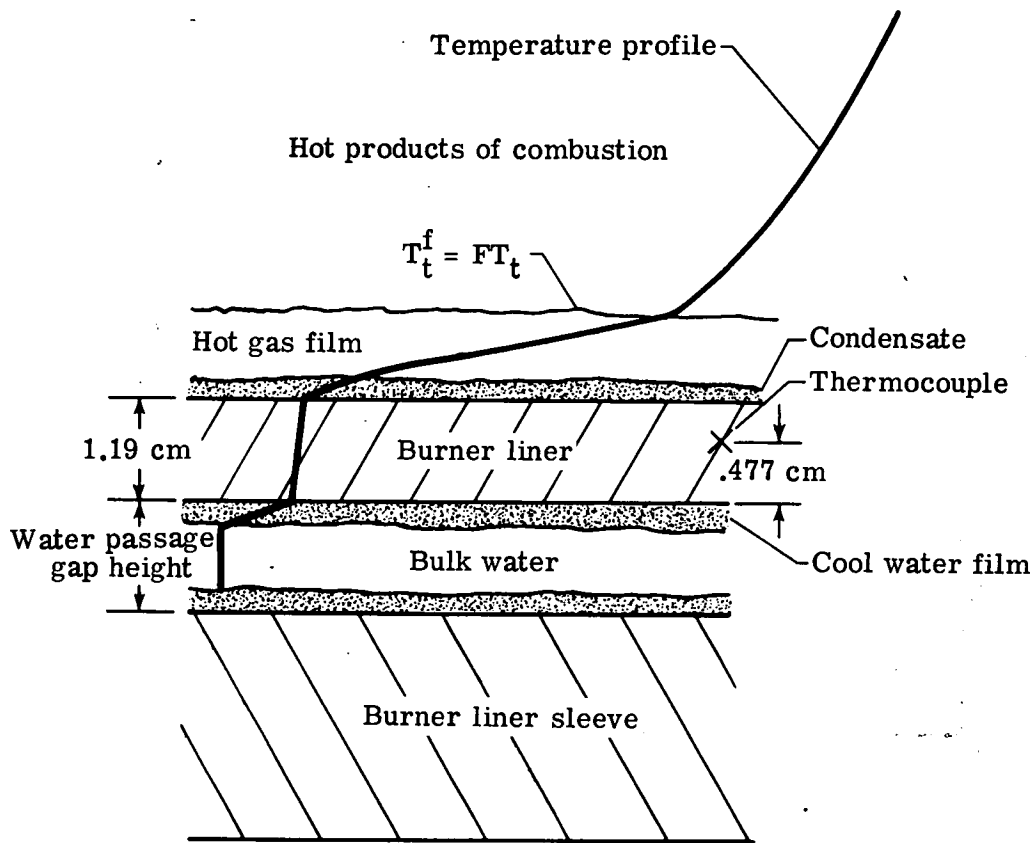


Figure 32.- Heat-transfer model.

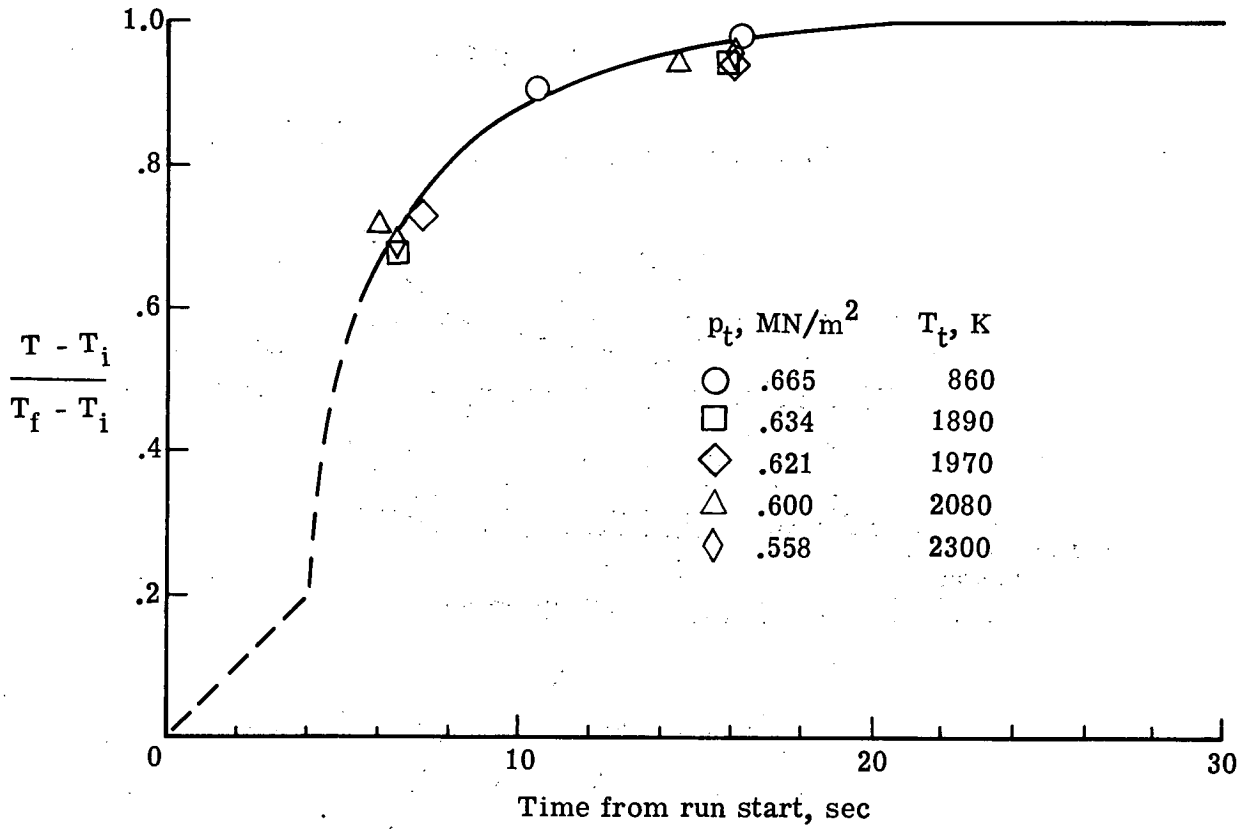


Figure 32.- Time history of burner liner temperature. Test 72.

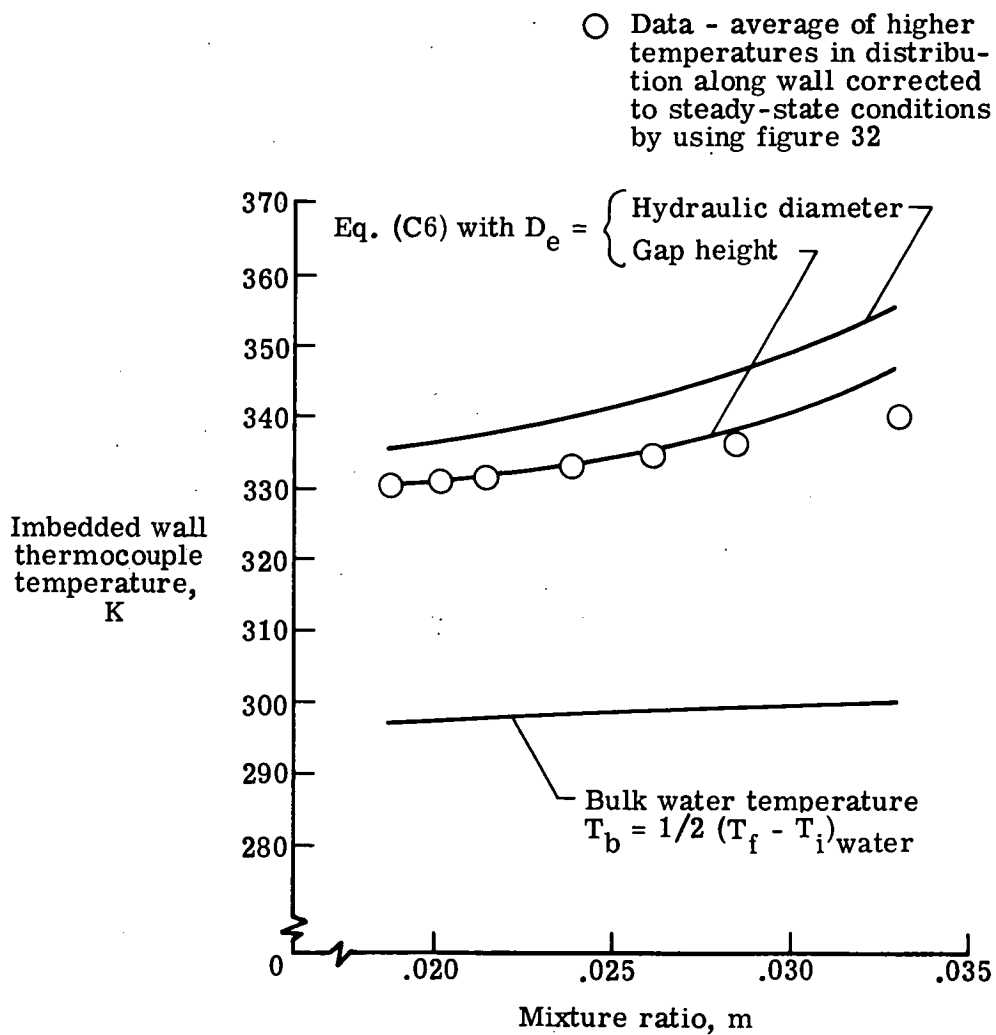


Figure 34.- Comparison of cold-side heat-transfer theory with experimental data. Test 55.

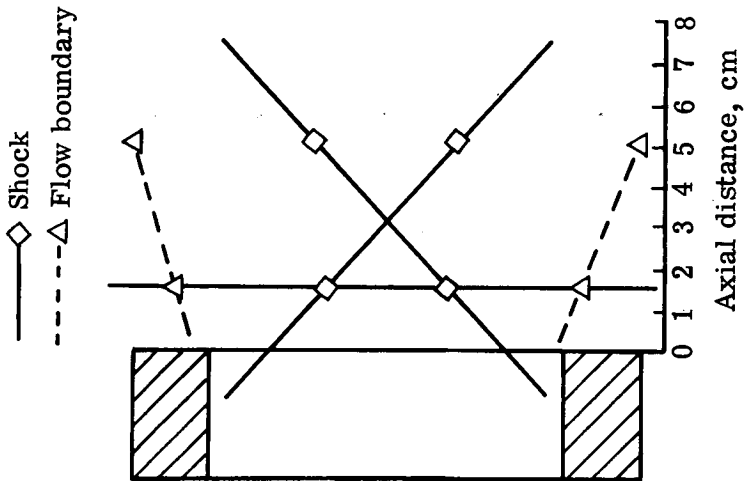
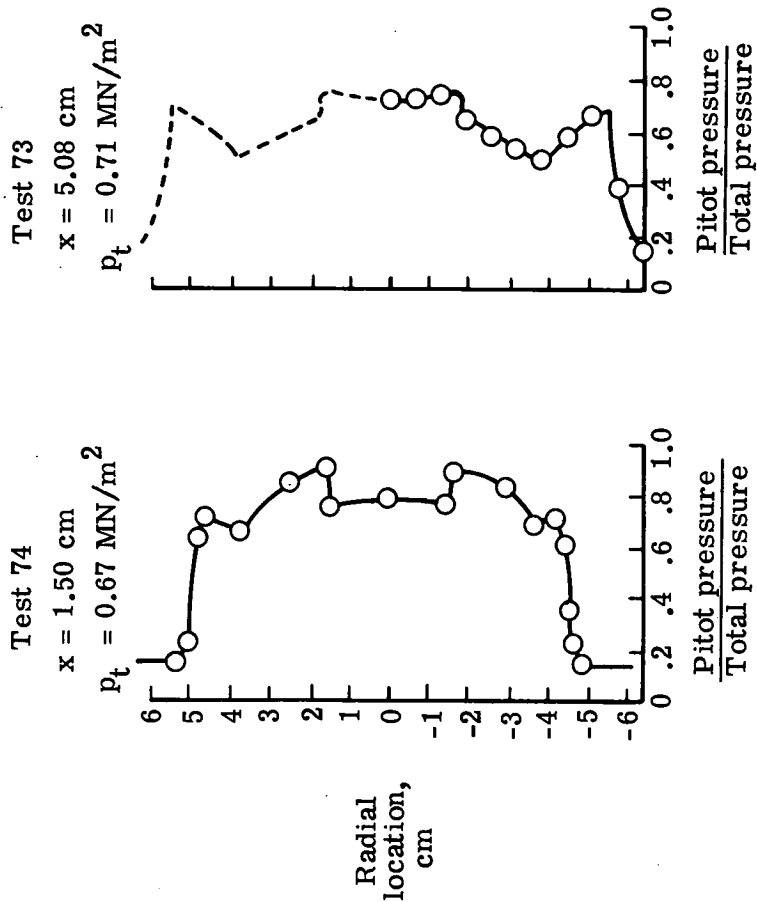


Figure 35.- Exhaust gas flow model and pitot pressure profiles.



POSTMASTER : If Undeliverable (Section 158
Postal Manual) Do Not Return

"The aeronautical and space activities of the United States shall be conducted so as to contribute . . . to the expansion of human knowledge of phenomena in the atmosphere and space. The Administration shall provide for the widest practicable and appropriate dissemination of information concerning its activities and the results thereof."

—NATIONAL AERONAUTICS AND SPACE ACT OF 1958

NASA SCIENTIFIC AND TECHNICAL PUBLICATIONS

TECHNICAL REPORTS: Scientific and technical information considered important, complete, and a lasting contribution to existing knowledge.

TECHNICAL NOTES: Information less broad in scope but nevertheless of importance as a contribution to existing knowledge.

TECHNICAL MEMORANDUMS: Information receiving limited distribution because of preliminary data, security classification, or other reasons. Also includes conference proceedings with either limited or unlimited distribution.

CONTRACTOR REPORTS: Scientific and technical information generated under a NASA contract or grant and considered an important contribution to existing knowledge.

TECHNICAL TRANSLATIONS: Information published in a foreign language considered to merit NASA distribution in English.

SPECIAL PUBLICATIONS: Information derived from or of value to NASA activities. Publications include final reports of major projects, monographs, data compilations, handbooks, sourcebooks, and special bibliographies.

TECHNOLOGY UTILIZATION PUBLICATIONS: Information on technology used by NASA that may be of particular interest in commercial and other non-aerospace applications. Publications include Tech Briefs, Technology Utilization Reports and Technology Surveys.

Details on the availability of these publications may be obtained from:

SCIENTIFIC AND TECHNICAL INFORMATION OFFICE

NATIONAL AERONAUTICS AND SPACE ADMINISTRATION

Washington, D.C. 20546